iScience

CellPress

Article

KDM3A and KDM4C Regulate Mesenchymal Stromal Cell Senescence and Bone Aging via Condensin-mediated Heterochromatin Reorganization

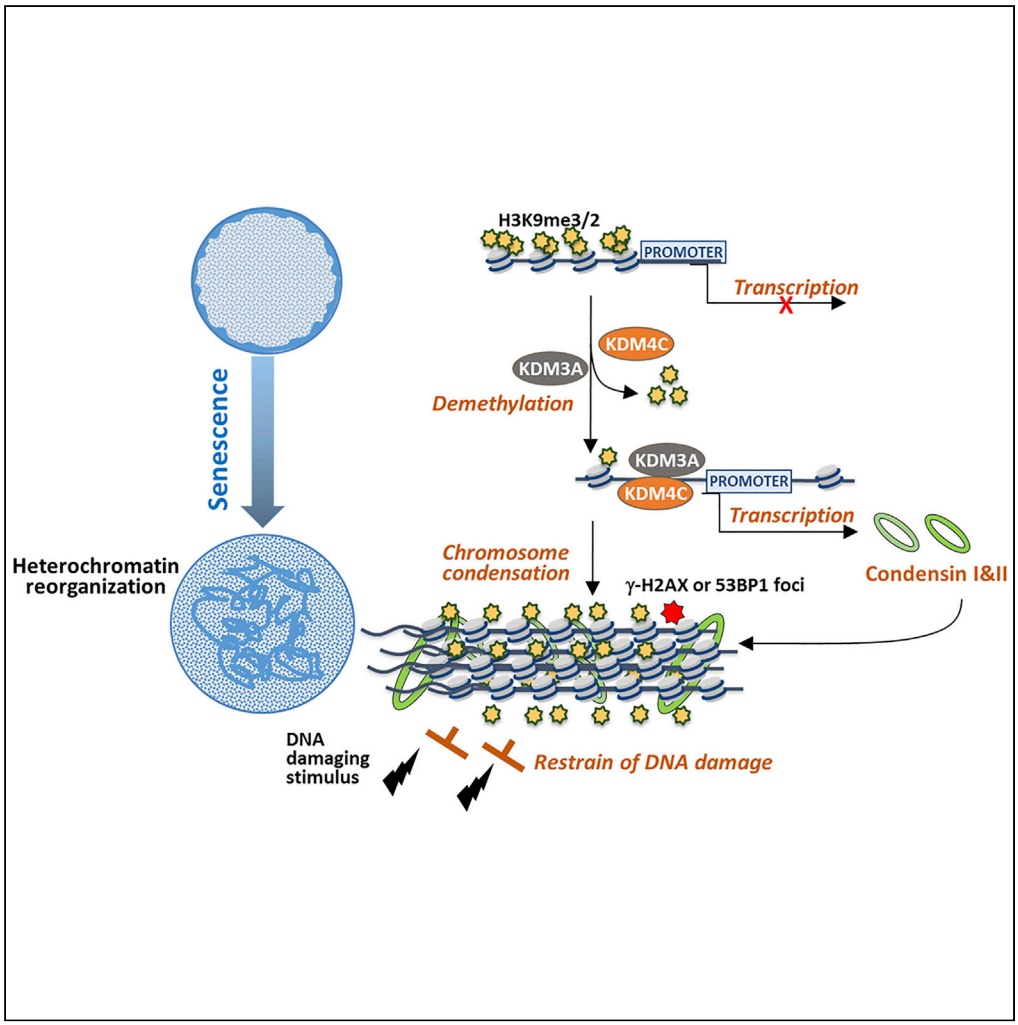

Biao Huang, Bin Wang, Wayne Yuk-Wai Lee, ..., Hsiao Chang Chan, Gang Li, Xiaohua Jiang

xjiang@cuhk.edu.hk

HIGHLIGHTS

KDM3A and KDM4C restrain DNA damage response during MSC senescence

KDM3A and KDM4C promote heterochromatin reorganization via induction of condensin

Loss of *Kdm3a* exacerbates MSC senescence and bone aging in mice

Chronological aging of human MSCs is associated with reduced expression of KDM3A and KDM4C

Huang et al., iScience *21*, 375–390
November 22, 2019
https://doi.org/10.1016/j.isci.2019.10.041

iScience

CellPress

Article

KDM3A and KDM4C Regulate Mesenchymal Stromal Cell Senescence and Bone Aging via Condensin-mediated Heterochromatin Reorganization

Biao Huang,[1,2] Bin Wang,[2,3] Wayne Yuk-Wai Lee,[2,3] Kin Pong U,[1,2] Kam Tong Leung,[4] Xican Li,[5,6] Zhenqing Liu,[1] Rui Chen,[1] Jia cheng Lin,[1,2] Lai Ling Tsang,[1,2] Baohua Liu,[7] Ye chun Ruan,[8] Hsiao Chang Chan,[1,2] Gang Li,[2,3] and Xiaohua Jiang[1,2,9,*]

SUMMARY

Epigenomic changes and stem cell deterioration are two hallmarks of aging. Accumulating evidence suggest that senescence of mesenchymal stromal cells (MSCs) perpetuates aging or age-related diseases. Here we report that two H3K9 demethylases, *KDM3A* and *KDM4C*, regulate heterochromatin reorganization *via* transcriptionally activating condensin components *NCAPD2* and *NCAPG2* during MSC senescence. Suppression of KDM3A or KDM4C by either genetic or biochemical approach leads to robust DNA damage response and aggravates cellular senescence, whereas overexpression of *KDM3A/KDM4C* or NCAPD2 promotes heterochromatin reorganization and blunts DNA damage response. Moreover, MSCs derived from *Kdm3a*−/− mice exhibit defective chromosome organization and exacerbated DNA damage response, which are associated with accelerated bone aging. Consistently, analysis of human bone marrow MSCs and transcriptome database reveals inverse correlation of KDM3A/KDM4C and/or NCAPD2/NCAPG2 with aging. Taken together, the present finding unveils that H3K9 demethylases function as a surveillance mechanism to restrain DNA damage accumulation in stem cells during aging.

INTRODUCTION

Aging is a complex multifactorial biological process manifested by a gradual decline of normal physiological functions in a time-dependent manner. The accumulation of senescent cells in aged tissues has been recognized as one of the most important common denominators of aging (Lopez-Otin et al., 2013). Mesenchymal stromal cells (MSCs) are extremely important adult stem cells for tissue homeostasis, regeneration, and repair. Despite their importance, it should be noted that MSCs are particularly sensitive to aging and age-related diseases, due to their central integration in the body (Baker et al., 2015). In fact, the regenerative capacity of bone marrow MSCs deteriorates after 30 years old (Caplan, 2005), and their deterioration has been recognized as an important hallmark of aging (Boyette and Tuan, 2014; Lopez-Otin et al., 2013). Reciprocally, MSC senescence contributes to the pathogenesis of age-related diseases, such as osteoporosis and osteoarthritis (Patel et al., 2016). Multiple signaling pathways leading to cellular senescence including p53/p21, p16/RB, and Akt/mTOR have been implicated in MSC senescence, which cause permanent cell cycle withdrawal and irreversible damage in very old MSCs (Gharibi et al., 2014; Lin et al., 2014; Wong et al., 2015; Yu and Kang, 2013). However, unlike a static endpoint, senescence reflects a series of progressive and phenotypically diverse cellular states acquired after the initial growth decline (Boyette and Tuan, 2014; Turinetto et al., 2016; Yu and Kang, 2013). A deeper understanding of the molecular mechanisms underlying the multi-step progression of MSC senescence and the link between MSC senescence and organism aging may lead to new therapeutic strategies for age-related diseases.

One striking characteristic of senescent cells is the large-scale alteration of genome architecture. For instance, in oncogene-induced senescence in fibroblasts, accumulation of constitutive heterochromatin and a dramatic rearrangement of heterochromatin into foci have been well documented (Hebbar et al., 2017; Narita et al., 2003). In contrast, a loss of heterochromatin has been described in replicative senescence and premature aging (progeroid) syndromes (Collinson et al., 2016; Goldman et al., 2004; Mani et al., 2017). The disparate nuclear phenotypes that accompany the different stress responses might be simply explained by the differences between acute and chronic senescence models (Chandra and Kirschner, 2016). Although the physiological function and molecular mechanism underlying the heterochromatin

[1]Key Laboratory for Regenerative Medicine of the Ministry of Education of China, School of Biomedical Sciences, Faculty of Medicine, The Chinese University of Hong Kong, Room 409A, Lo Kwee Seong Integrated Biomedical Sciences Building, Area 39, Shatin, Hong Kong SAR, PR China

[2]The Chinese University of Hong Kong, Shenzhen Research Institute, Shenzhen, PR China

[3]Department of Orthopaedics & Traumatology, Faculty of Medicine, The Chinese University of Hong Kong, Hong Kong SAR, PR China

[4]Department of Pediatrics, Faculty of Medicine, The Chinese University of Hong Kong, Hong Kong SAR, PR China

[5]School of Chinese Herbal Medicine, Guangzhou University of Chinese Medicine, Guangzhou 510006, China

[6]Innovative Research & Development Laboratory of TCM, Guangzhou University of Chinese Medicine, Guangzhou 510006, China

[7]Shenzhen University Health Science Center, Shenzhen University, Shenzhen, PR China

[8]Department of Biomedical Engineering, The Hong Kong Polytechnic University, Hong Kong, PR China

[9]Lead Contact

*Correspondence: xjiang@cuhk.edu.hk

https://doi.org/10.1016/j.isci.2019.10.041

reorganization during senescence is still elusive, it should be noted that recent study demonstrated that MSCs derived from *WRN* null (−/−) embryonic stem cells displayed a pronounced senescence phenotype, which was attributed to disorganized heterochromatin (Zhang et al., 2015), raising a possibility that the unique and organized change of heterochromatin landscape functions as a protective mechanism against cellular senescence. Heterochromatin is characterized by typical post-translational modifications on histones, which have been postulated to be one of the mechanisms to facilitate the folding of heterochromatin into highly condensed structures (Benayoun et al., 2015; Chandra et al., 2015; Chandra and Narita, 2013; Ugarte et al., 2015; Zhu et al., 2013). These regions of compacted and transcriptionally repressive chromatin are critical for diverse aspects of nuclear biology, including the regulation of gene expression, the transcriptional silencing of genomic repeats, DNA repair, and the maintenance of genome stability (Bulut-Karslioglu et al., 2014). Methylation of histone H3 at lysine 9 has a well-recognized role in the establishment and maintenance of heterochromatin structure (Benayoun et al., 2015; Ugarte et al., 2015; Zhu et al., 2013). SUV39H1, the first-described H3K9 methyltransferase, has been associated with oncogene-induced senescence and pathological aging process (Braig et al., 2005; Peters et al., 2001); however, it is still unclear whether SUV39H1 regulates physiological aging. On the other hand, the steady state of methylation at H3 lysine 9 is dictated by the balance between addition and removal of methyl groups, which is achieved by a reciprocal action between lysine methyltransferases (KMTs) and histone demethylases (KDMs) (Munoz-Espin and Serrano, 2014). Indeed, several recent studies have provided experimental evidence that KDMs are involved in the longevity regulation in *Caenorhabditis elegans* (Johmura et al., 2016; Merkwirth et al., 2016; Sen et al., 2015), indicating the potential role of KDMs in cellular senescence and organism aging.

H3K9 demethylation is mainly catalyzed by Fe(II)- and α-ketoglutarate-dependent JmjC-domain-containing proteins, including the JMJD1/KDM3 family, JMJD2/KDM4 family, and PHF8/KDM7B (Mosammaparast and Shi, 2010). In this study, we identify two conserved H3K9 KDMs, KDM3A and KDM4C, that regulate heterochromatin reorganization to restrain DNA damage and progression of MSC senescence via transcriptionally activating condensin components *NCAPD2* and *NCAPG2*. Decline in KDM3A and/or KDM4C leads to aggravated MSC senescence and bone aging in mice and is significantly correlated with chronological aging of MSCs in human. Our finding thus unveils a protective role of KDM-mediated heterochromatin reorganization in stem cells, which may provide potential targets for the diagnosis and intervention of age-related diseases.

RESULTS

MSC Senescence Is Accompanied by Heterochromatin Reorganization

To experimentally assess MSC senescence *in vitro*, we established a replicative senescence model using either human bone marrow stromal cells (hBMSCs) or human umbilical cord-derived stromal cells (hUCMSCs). Late passage hMSCs presented typical phenotypes of cellular senescence, including increased β-galactosidase (SA-β-gal) activity, reduced colony forming ability, loss of proliferative potential, and upregulation of $p21^{WAF1}$ (Figure S1A). To further evaluate the dynamic change of heterochromatin and H3K9 methylation accompanied by hMSC senescence, we focused on hUCMSCs, which sustains rapid multiplication until p16-p18 (Chen et al., 2015). A gradual aging process in hUCMSCs was demonstrated by progressively increased SA-β-gal–positive cells (Figure 1A). In consistence with the previous reports, the expression levels of H3K9 methylation and heterochromatin mark HP1-γ were dramatically reduced at the final stage of cellular senescence (p26), at which more than 85% of cells reached a senescence state (Figures 1A and 1B, p26). Of note, although the expression levels of H3K9 methylation were eventually lost, there was a mild induction of these repressive heterochromatin marks at the early stage of senescence (p10-p16) at which only small amount of cells exhibited senescent features (Figures 1B and S1B). The induction of heterochromatin marks was further validated by immunofluorescent staining using constitutive heterochromatin mark H3K9me3 and a centromere-specific heterochromatin mark CENPA (Figure 1C). In the young hUCMSCs (p6), heterochromatin was mainly localized underneath the nuclear membrane. On senescence entry, heterochromatin was markedly increased and reorganized into condensed heterochromatin foci (p16). Collectively, these data demonstrate that MSC senescence is accompanied by heterochromatin reorganization.

Identification of H3K9 Demethylases KDM3A and KDM4C that Are Potentially Involved in MSC Senescence

Post-translational modifications of histones such as methylation and acetylation are central in the regulation of heterochromatin structure. To investigate the potential roles of histone modification in

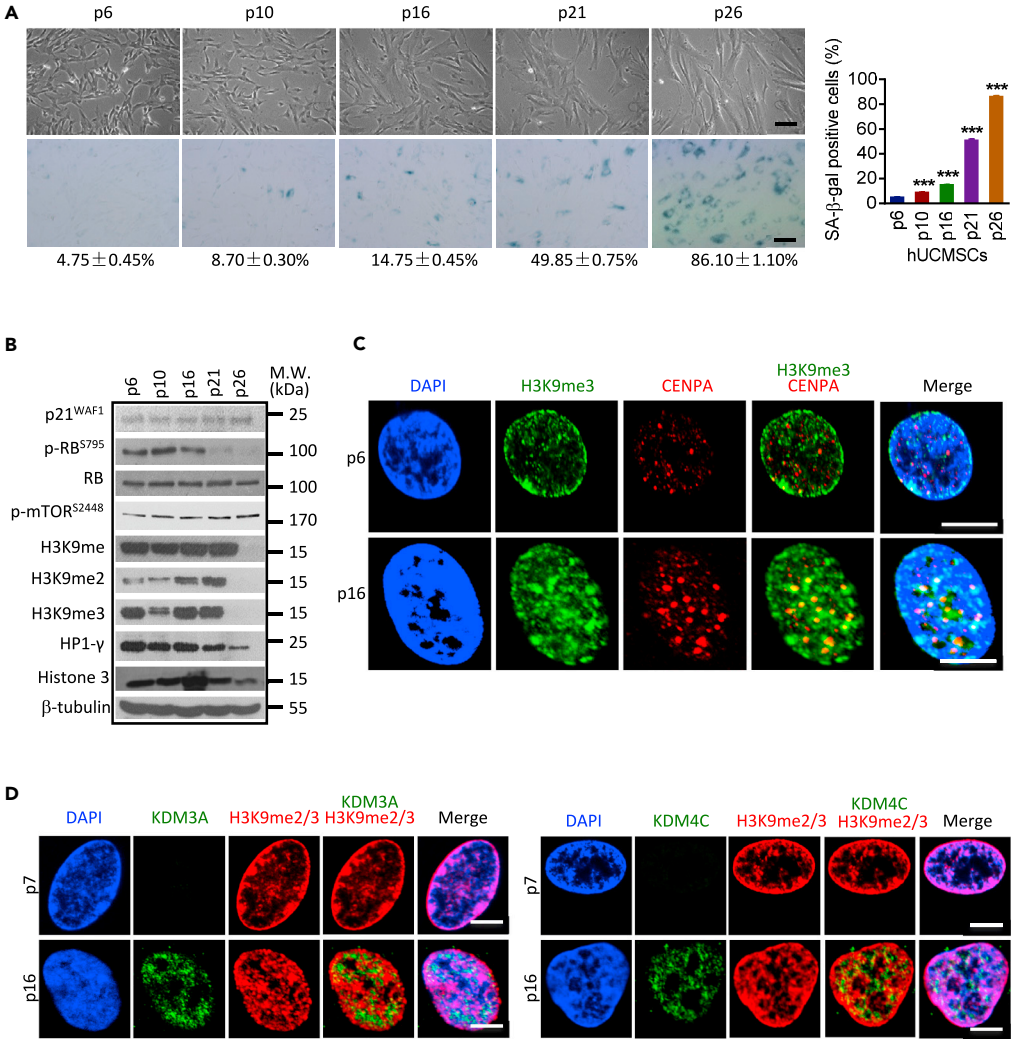

Figure 1. MSC Senescence Is Accompanied by Heterochromatin Reorganization

Three hUCMSCs lines (hUC009, hUC011, hUC013) were used for serial passaging and characterized with various senescence markers.

(A)Morphology and β-Gal staining (scale bar = 100μm) in serial passage replicative senescence cell model with hUCMSCs. Quantification is shown at the right panel; data are presented as the mean ± SEM. ***$p < 0.01$ (t test, n = 3).

(B) Representative Western blot showing the expression levels of senescence marker genes and heterochromatin marks along with hUCMSCs aging; experiments were repeated three times.

(C) Representative images of immunofluorescence staining with H3K9me3 (green) and CENPA (red) in hUCMSCs at passage 6 and 16 (scale bar = 10μm). Experiments were repeated at least three times using three different hUCMSCs lines.

(D) Representative images of immunofluorescence staining of KDM3A or KDM4C and H3K9me2/3 in hUCMSCs at p7 and p16 (scale bar = 10μm). Experiments were repeated at least three times using three different hUCMSCs lines.

heterochromatin reorganization and MSC senescence, we profiled the expression of histone modifying enzymes using both replicative senescence model (hBMSCs and hUCMSCs) and chronological aging model (rat primary young *Vs* old BMSCs) (Figure S1C). The screening results showed that the mRNA expression levels of KDM3A, KDM4C, and KDM5C were consistently upregulated, whereas *SUV39H1* was consistently downregulated in the three models (Figures S2A–S2D). Of note, both KDM3A and KDM4C and SUV39H1 target on H3K9 methylation. We decided to focus on the two H3K9 KDMs, because the role of KDMs in stem cell senescence has not been characterized. The immunofluorescent staining and Western blot revealed that both KDM3A and KDM4C were readily upregulated at the early stage of senescence when heterochromatin is reorganized (Figures 1D and S2E).

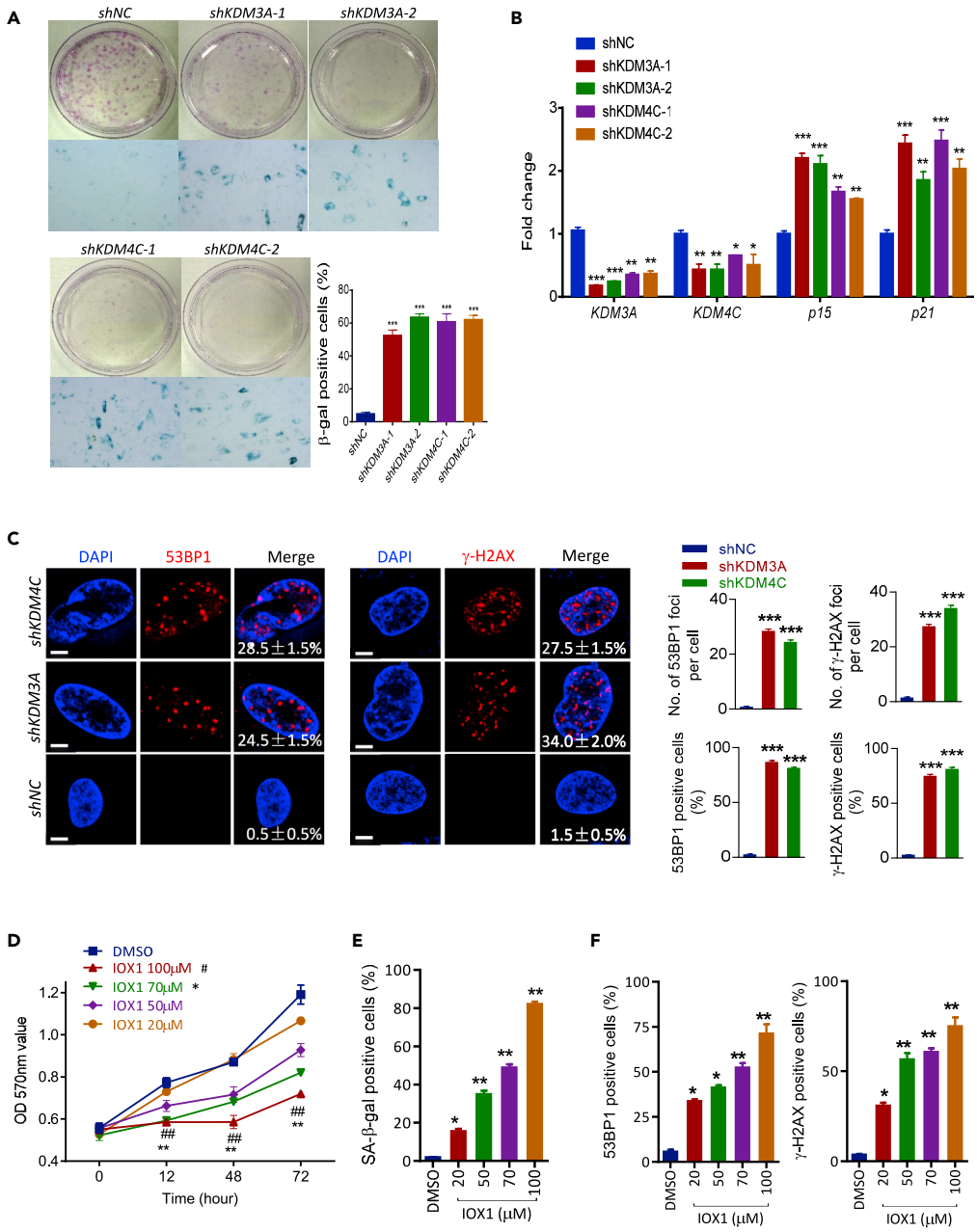

Figure 2. Suppression of H3K9 Demethylases KDM3A and KDM4C Induces DNA Damage and Accelerates Cellular Senescence in hUCMSCs

Two different hUCMSCs lines (hUC009, hUC013) were used for knockdown or IOX experiments.

(A) Representative images of colony formation and β-Gal staining (scale bar = 100μm) in hUCMSCs treated with control shRNA or shRNAs targeting *KDM3A* or *KDM4C*. The cells were selected by ZsGreen positivity after lentiviral transduction and grew for two more passages. Quantification of β-Gal staining is shown at the right; data are presented as the mean ± SEM. ***p < 0.001 (t test: n = 3).

(B) RT-qPCR assay showing the expression levels of *KDM3A*, *KDM4C*, *p15*, and *p21* after shRNA treatment; data are presented as the mean ± SEM. **p < 0.01; ***p < 0.001 (t test: n = 3).

(C) Representative images (scale bar = 5μm) and quantification of 53BP1, γ-H2AX foci in hUCMSCs transduced with lentiviral particles carrying shKDM3A-1, shKDM4C-1, or control shRNA. Quantification data are presented as mean ± SEM of values from three independent experiments with triplicate wells analyzed on 6–8 cells/field from five different fields. ***p < 0.001 (t test).

Figure 2. *Continued*

(D) MTT assay of hUCMSCs (p6) treated with different concentrations of IOX1 or DMSO for 72 h. Data are presented as the mean ± SEM of values from three independent experiments; **p < 0.01, IOX70μM compared with control; ##p < 0.01, IOX100μM compared to control group (t test).

(E) Quantification of β-Gal staining in hUCMSCs (p7) treated with different concentrations of IOX1 (20, 50, 70, and 100 μM). Data are presented as the mean ± SEM. *p < 0.05; **p < 0.01 (one-way ANOVA, n = 3).

(F) Quantification of 53BP1 and γ-H2AX foci in hUCMSCs (p6) treated with different concentration IOX1 (20, 50, 70, and 100 μM) and DMSO control. Quantification is shown at the right; mean ± SEM of values from three independent experiments with triplicate wells analyzed on 6–8 cells/field from five different fields. *p < 0.05; **p < 0.01 (one-way ANOVA).

To further investigate the potential role of KDM3A and KDM4C in heterochromatin reorganization and MSC senescence, we knocked down *KDM3A* or *KDM4C* using shRNA (Figure S3A) in the early passage hUCMSCs (p6). Our results showed that suppression of *KDM3A* or *KDM4C* induced a rapid onset of cellular senescence (p8) as demonstrated by increased β-gal activity, reduced colony formation, and increased expression of *p21* and *p15* in hUCMSCs (Figures 2A and 2B). Of particular interest, knockdown of *KDM3A* or *KDM4C* provoked a robust increase of γ-H2AX and 53BP1 foci, indicating an accumulation of DNA damage response (DDR) (Figure 2C). To answer the question of whether the effects of KDM3A and KDM4C on cellular senescence and DDR are related to their function as H3K9 demethylase, we used IOX1, a specific JmjC histone demethylase inhibitor, to treat hUCMSCs at p6-p8. In corroboration with the knockdown data, IOX1 treatment suppressed cell proliferation, increased β-gal activity, and enhanced DDR in a dose-dependent manner (Figures 2D–2F, S3B, and S3C). These results suggest that KDM3A and KDM4C protect MSCs from cellular senescence and DDR, the effect of which is related to their histone demethylase activity.

KDM3A and KDM4C Regulate Condensin Complex Components NCAPD2 and NCAPG2 via Their Demethylase Activity

To elucidate the mechanism underlying the regulatory effect of KDM3A and KDM4C on MSC senescence, we analyzed the KDM3A- or KDM4C-dependent transcriptional program using RNA-seq in MSCs. Manipulation of *KDM3A* or *KDM4C* led to a consistent change in chromosome organization genes, in particular chromosome condensation genes (Figures S4A and S4B, GEO: GSE133098). Interestingly, among the chromosome condensation genes, we have identified that various components of the condensin complex I and II are consistently downregulated in *KDM3A*- or *KDM4C*-knockdown hUCMSCs or upregulated in *KDM3A* or *KDM4C*-overexpressing hUCMSCs (Figures 3A and S4B). We decided to focus on *NCAPD2* and *NCAPG2*, the major components of condensin I and condensin II, respectively, which are unanimously regulated by KDM3A and KDM4C. Our real-time PCR and Western blot showed that siRNA knockdown of either *KDM3A* or *KDM4C* reduced the expression levels of both NCAPD2 and NCAPG2 (Figures 3B and S4C). Moreover, the binding of KDM3A and KDM4C on the promoter of *NCAPD2* was significantly downregulated, whereas the occupancy of corresponding H3K9me3 and H3K9me2 was significantly upregulated in knockdown hUCMSCs (Figure 3C). In addition, inhibition of H3K9 demethylase activity by IOX1 reduced the expression levels of NCAPD2 and NCAPG2 (Figure 3D). IOX1 also reduced the expression level of Lamin B1 and increased the expression level of p53, supporting the senescence-inducing property of IOX1. The regulatory effect of IOX1 was attributed to the enzyme inhibitory function, as IOX1 increased the enrichment of H3K9me2 and H3K9me3 on *NCAPD2* promoter (Figure 3E). Altogether, these data clearly indicate that KDM3A and KDM4C function as positive transcriptional regulators of condensin components via their H3K9 demethylase activity. As a first step to identify the potential mechanism underlying condensin-mediated effects, quantitative ChIP-PCR was used to determine the recruitment of NCAPD2 on repetitive DNA sequences, at which heterochromatin enriches. Our results showed that the binding of NCAPD2 on replicative DNA sequences was significantly reduced in *KDM3A*- or *KDM4C*-knockdown cells (Figure 3F), suggesting that KDM-mediated regulation of condensin might be critical for stabilizing the heterochromatin structure during senescence.

KDM3A and KDM4C Induce Heterochromatin Reorganization to Restrain DNA Damage Response in Doxorubicin-Induced Senescence

The finding that suppression of KDM3A and KDM4C leads to increased DDR raises the possibility that KDM3A and KDM4C function as a protective mechanism against DNA damage during cellular senescence. To establish a direct link between KDM3A/KDM4C and DDR in senescent cells, we applied a DNA damage–induced acute senescence model in hUCMSCs using Doxorubicin (DOX). DOX treatment

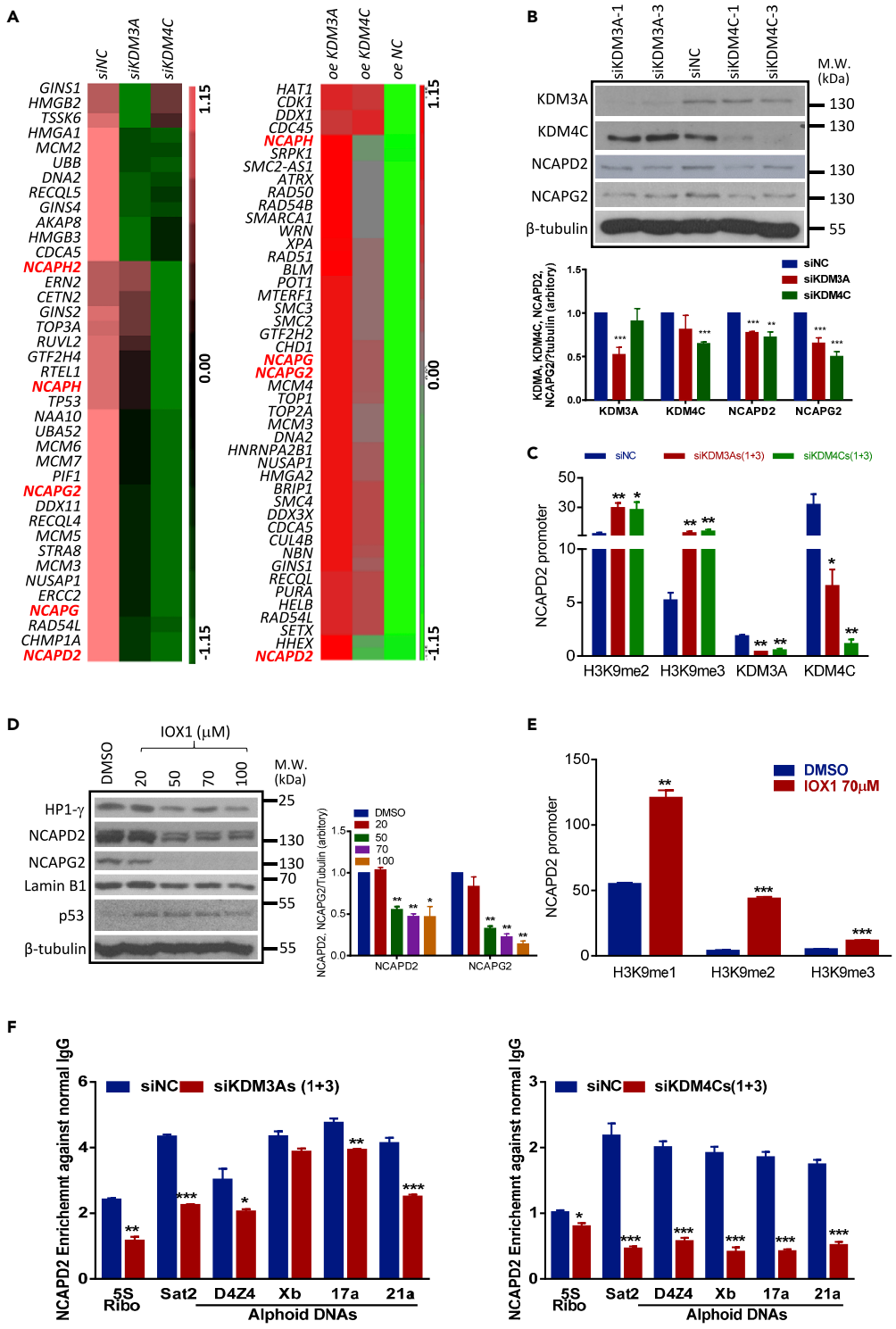

Figure 3. KDM3A and KDM4C Transcriptionally Regulate Condensin Components NCAPD2 and NCAPG2 via Their Demethylase Activity

(A) Heatmap showing the global downregulation and upregulation of chromosome condensation genes in siKDM3A-/siKDM4C-knockdown (hUC009) or KDM3A-/KDM4C-overexpressing hUCMSCs (hUC013) compared with their relative control hUCMSCs.

Figure 3. *Continued*

(B) Representative Western blot showing that the expression levels of NCAPD2 and NCAPG2 are downregulated in *KDM3A*- or *KDM4C*-knockdown cells (hUC009). Data are presented as the mean ± SEM. **p < 0.01; ***p < 0.001 (t test).

(C) ChIP-qPCR showing the enrichment of H3K9me2, 3, *KDM3A* (siKDM3A-1+siKDM3A-3), or *KDM4C* (siKDM4C-1+siKDM4C-3) on *NCAPD2* promoters relative to IgG enrichment after siRNA treatment. Data are presented as the mean ± SEM. *p < 0.05; **p < 0.01 (t test, n = 3).

(D) Representative Western blot showing the expression of senescence markers and NCAPD2 and NCAPG2 in hUCMSCs (p6-p8) treated with different concentration IOX1 (20, 50, 70, and 100μM). Experiments were repeated three times with two hUCMSCs lines (hUC009, hUC013). Data are presented as the mean ± SEM. *p < 0.05; **p < 0.01 (one-way ANOVA).

(E) ChIP-qPCR showing increased enrichment of H3K9me1, 2, and3 on the representative *NCAPD2* promoter relative to IgG enrichment in 70μM IOX1-treated hUCMSCs. Data are presented as the mean ± SEM. **p < 0.01; ***p < 0.001 (t test: n = 3).

(F) ChIP-qPCR showing the enrichment of NCAPD2 on several repetitive DNA sequences loci in control- or *KDM3A* (siKDM3A-1+siKDM3A-3) or *KDM4C* (siKDM4C-1+siKDM4C-3) siRNA-treated hUCMSCs, data are presented as the mean ± SEM, *p < 0.05; **p < 0.01;
***p < 0.001 (t test: n = 3).

induced a gradual increase in KDM3A and KDM4C level peaked at 10–12 h, which thereafter decreased at 24 h and returned to virtually background level at 48 h. Of note, the kinetics of heterochromatin marks H3K9me3 and HP1γ, and condensin components NCAPD2 and NCAPG2 were consistent with the KDMs upon DOX treatment (Figure 4A), suggesting DOX treatment induces a heterochromatin reorganization process, which may be associated with KDM3A and KDM4C. In corroboration with the Western blot result, the immunofluorescent staining showed that heterochromatin mark gradually increased, which peaked at 10 h and decreased thereafter. Accordingly, 53BP1 and γ-H2AX foci were induced at 24 h, which stochastically distributed throughout the nucleus, and maximized around 48 h after DNA damage (Figures 4B and 4C). The sequential inductive effect on heterochromatin reorganization and DDR upon DOX treatment suggests a surveillance mechanism by heterochromatin rearrangement. In fact, knockdown of *KDM3A* and *KDM4C* or treatment with IOX1 markedly aggravated DOX-induced DDR and cellular senescence (Figures 4D, S5A, and S5B). By contrast, overexpression of *KDM3A* or *KDM4C* significantly reduced the number of DOX-induced 53BP1 and γ-H2AX foci and degree of cellular senescence as demonstrated by decreased β-gal activity and a dramatic downregulation of $p21^{WAF1}$ (Figures 4E, S5C, and S5D). In addition, overexpression of condensin I complex component *NCAPD2* alone significantly rescued DOX-induced DDR and cellular senescence, albeit at a lower level compared with *KDM3A* or *KDM4C* overexpression (Figures 4E, S5C, and S5D). The protective role of KDM3A and KDM4C is related to heterochromatin reorganization, as overexpression of *KDM3A*/*KDM4C* or *NCAPD2* promoted heterochromatin reorganization as indicated by H3K9me2/3 staining (Figures S5C and S5D). The role of KDM3A/KDM4C and NCAPD2 in chromatin reorganization was further illustrated by Transmission Electron Microscope (TEM) analysis or immunofluorescent staining in *KDM3A*/*KDM4C*- or *NCAPD2*-overexpressing cells. As shown in Figure S6A, *KDM3A* or *KDM4C* overexpression induced chromosome condensation in the nuclear. Similarly, overexpression of *NCAPD2* directly promoted heterochromatin reorganization as indicated by an increase of H3K9me3 positive foci (Figure S6B). Collectively, these results clearly demonstrate a protective role of KDM3A and KDM4C in DNA damage–induced senescence through induction of heterochromatin reorganization.

Dynamic Change of KDM3A/KDM4C and Condensin Complex Components during Bone Aging in Mice

Having established the role of KDM3A and KDM4C in MSC senescence *in vitro*, we asked whether the two H3K9 KDMs are related to heterochromatin reorganization of MSCs during aging *in vivo*. For this purpose, we established ovariectomized (OVX) rat model, which is a well-established model to study bone aging process. Successful OVX was validated at sacrifice, using uterus weight, bone CT, and morphometric indexes (Figures S7A–S7C). We then isolated rat bone marrow MSCs (rBMSCs) at different time points starting from 3 weeks to 12 weeks after OVX and determined the molecular changes and heterochromatin marks indicative of cellular senescence. The result illustrated a dramatic reduction of H3K9 methylation in rBMSCs collected at 9–12 weeks, at which the osteoporosis was utmost severe (Figure 5A). Of note, the kinetics of *Kdm3a* and *Kdm4c* expression peaked at both 6 weeks and 12 weeks (Figures 5A and 5B) recapitulating the expression dynamics in replicative senescence model (Figure S2E). Importantly, a gradual increase of senescence markers including *p15*, *p19*, and *p27* was detected in rBMSCs along with disease development, indicating deterioration of rBMSCs along with bone aging process (Figure 5C). In addition, the expression

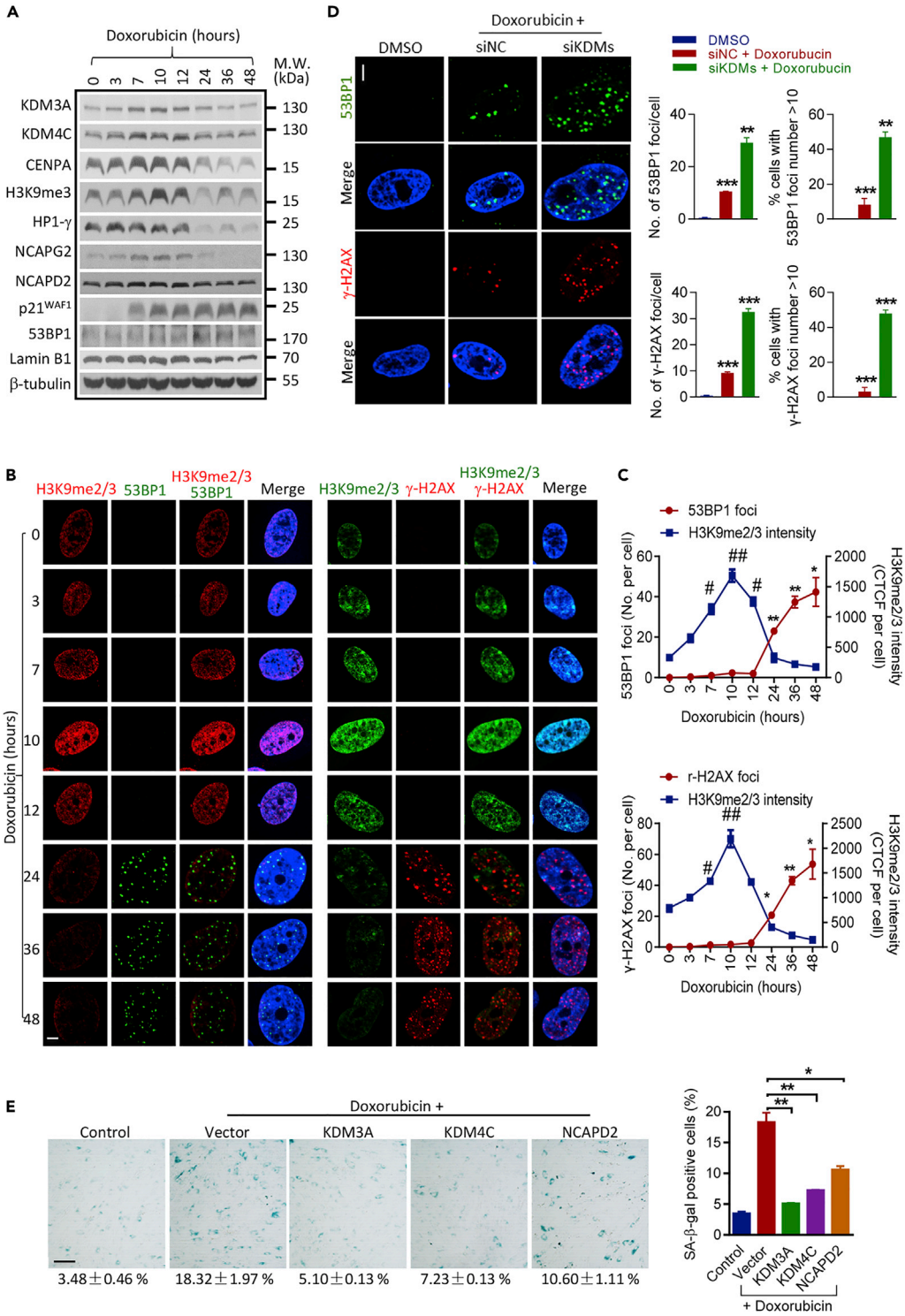

Figure 4. Doxorubicin Induces Heterochromatin Reorganization and DNA Damage Response

Two hUCMSCs lines (hUC009, hUC013) were used for Doxorubicin-induced cellular senescence model.

(A) Early passage hUC-MSCs (p6-7) were treated with Doxorubicin for 48 h. Representative Western blot showing the expression levels of KDM3A, KDM4C, heterochromatin marks, NCAPD2, NCAPG2, and senescence marks at different time points (0–48 h) after Doxorubicin treatment.

Figure 4. *Continued*

(B) Representative immunofluorescence images of 53BP1 or γ-H2AX foci and H3K9me2/3 staining (scale bar = 5μm) in hUCMSCs treated with Doxorubicin for different time points.

(C) Quantification of 53BP1 or γ-H2AX and H3K9me2/3 immunofluorescence staining in hUCMSCs treated with Doxorubicin for different time points (CTCF, corrected total cell fluorescence). Data are presented as mean ± SEM of values from three different experiments with triplicate wells analyzed on 6–8 cells/field from five different fields; *p < 0.05; **p < 0.01, 53BP1, γ-H2AX compared with control group, #p < 0.05; ##p < 0.01, H3K9me2/3 compared with control group (Wilcoxon/Mann-Whitney test).

(D) Representative images and quantification of 53BP1 and γ-H2AX immunofluorescence staining (scale bar = 5μm) in Doxorubicin-treated hUCMSCs transfected with scrambled siRNAs or siRNA mixtures (siKDM3A-1 + siKDM4C-3). Data are presented as mean ± SEM of values from three different experiments with triplicate wells analyzed on 6–8 cells/field from five different fields; **p < 0.01; ***p < 0.001 (t test).

(E) Representative images and quantification of β-Gal staining (scale bar = 100μm) in control group or Doxorubicin-treated hUCMSCs transfected with Vector plasmid or *KDM3A*, *KDM4C*, or *NCAPD2* plasmid.

Data are presented as the mean ± SEM. *p < 0.05; **p < 0.01 (t test, n = 3).

levels of *Ncapd2* and *Ncapg2* reached the peak at 6 weeks, which was in line with *Kdm3a* and *Kdm4c* up-regulation and decreased thereafter (Figure 5C), emphasizing the association between *Kdm3a*/*Kdm4c* and condensin complexes at the early stage of bone aging.

Deficiency of *Kdm3a* Leads to MSC Senescence and Bone Aging in Mice

The *Kdm3a*$^{-/-}$ mice have defects in sex determination, lipid metabolism, and spermatogenesis (Kuroki et al., 2013; Liu et al., 2010; Tateishi et al., 2009); however, the relationship between *Kdm3a* deficiency and aging has not been investigated. In this study, we took advantage of *Kdm3a* knockout mice to evaluate the effect of *Kdm3a* deficiency on bone aging (Figure S7D). We collected bone tissues from WT and KO mice at different ages and found that although no difference exists between WT and KO young mice (2 month), KO mice at 6 months old exhibited evident bone aging phenotype (Figure 6A). The expression levels of senescence markers p53, p21, and p16 were dramatically increased, whereas the expression of PCNA was significantly decreased in KO bones. In addition, senescence nuclear markers such as Lamin B1, H3K9me3, and H3K27me3 and condensin components were dramatically downregulated in KO bones, indicating the correlation between bone aging and heterochromatin destruction *in vivo* (Figures 6B and 6C). Of note, the expression of Suv39h1 was slightly increased in KO mice. To further correlate these changes with BMSCs, we isolated primary BMSCs from WT and KO mice. Our results showed that condensin components were significantly downregulated in KO BMSCs compared with WT BMSCs. In contrast, the expression levels of senescence genes such as *p53*, *p21*, and *Gadd34* were significantly upregulated in KO BMSCs (Figure S7E). Moreover, when challenged with DOX, KO BMSCs elicited a much enhanced DDR as illustrated by increased expression of 53BP1 and p21 (Figure S7F). The specificity of the KO was validated by overexpressing *Kdm3a* in KO BMSCs, which showed that overexpression of *Kdm3a* completely rescued aggravated cellular senescence and increased DDR induced by DOX in KO cells (Figures S7G and S7H). In addition, overexpression of *Ncapd2* alleviated the DOX-induced cellular senescence and DDR in KO BMSCs (Figures 6D and 6E). Altogether, these results strongly indicate that *Kdm3a* deficiency aggravates DNA damage and cellular senescence in BMSCs, which eventually contributes to the bone aging phenotype in mice.

The Expression Levels of KDMs and Condensin Components Are Inversely Correlated with Human Aging

Previous studies on gene expression analysis of young versus old human BMSCs have revealed large amounts of age-associated molecular changes related to MSC adhesion, cell cycle regulation, migration, and cytokine secretion (Bustos et al., 2014; Wilson et al., 2010). However, whether MSC aging is associated with a global change of genes involved in chromosome organization is unknown. In this study, we asked whether KDM3A/KDM4C and condensin components could be related to physiological aging in human stem cells. We first compared the expression levels of KDM3A/KDM4C, condensin components, and heterochromatin marks in primary BMSCs derived from nine young (13- to 32-year-old) and five old (52- to 61-year-old) individuals (Figure 7A). Our Western blot result showed a marked downregulation of KDM3A and KDM4C protein associated with a decrease in H3K9me3 and PCNA in BMSCs derived from old individuals. Importantly, the expression of NCAPG2 and NCAPD2 was dramatically decreased in aged BMSCs as well. It should be noted that the expression of SUV39H1 did not change in old BMSCs. To confirm the correlation of *KDM3A/KDM4C* and *NCAPD2/NCAPG2* with aging, we examined publically available MSC gene expression datasets (GEO: GSE39540). GSE dataset analysis revealed that the

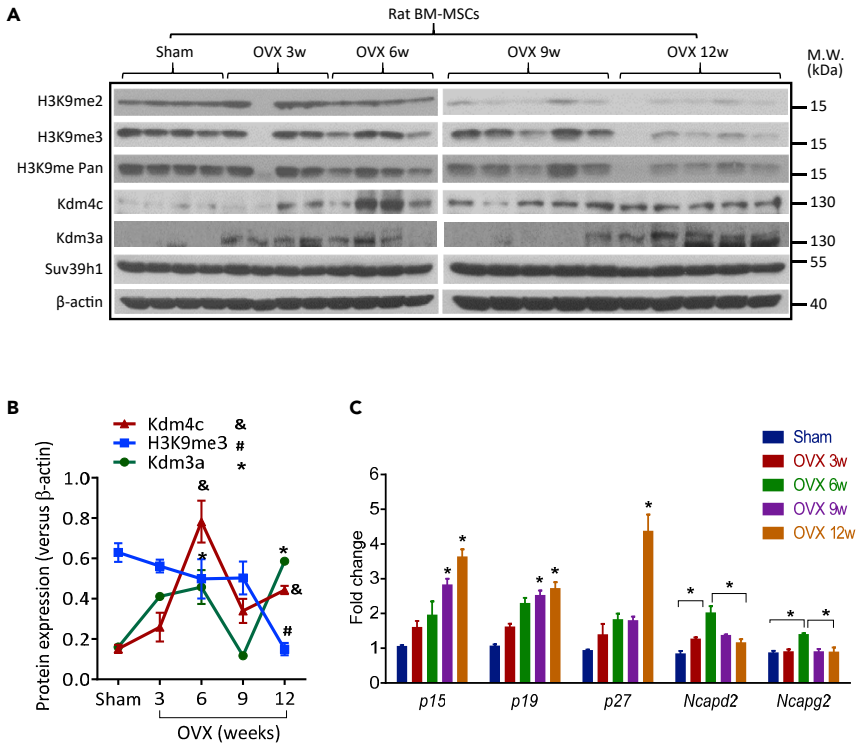

Figure 5. Dynamic Change of KDM3A and KDM4C in OVX Rat Model

(A) Western blot analysis of *Kdm3a*, *Kdm4c*, and H3K9 methylation in BMSCs derived from OVX rat model (total n = 22; Sham, n = 4; OVX3w, n = 4; OVX6w, n = 4; OVX9w, n = 5; OVX12w, n = 5). The experiments were repeated for three times.

(B) The quantification analysis of Western blot results of *Kdm3a*, *Kdm4c*, and H3K9me3 show two peaks of *Kdm3a* and *Kdm4c* (n = 22). *p < 0.05, change of *Kdm3a* expression compared with sham; p < 0.05, change of *Kdm4c* expression compared with sham; #p < 0.05, change of H3K9me3 compared with sham (Wilcoxon/Mann-Whitney test).

(C) RT-qPCR assay of *Ncapd2*, *Ncapg2*, and several cell cycle inhibitor genes in BMSCs derived from OVX rat model. Data are presented as mean ± SEM. *p < 0.05 (Wilcoxon/Mann-Whitney test, n = 22).

expression levels of *KDM3A*, *KDM4C*, *NCAPD2*, and *NCAPG2* were negatively correlated with human aging (Figure 7B). Taken together, these data clearly reveal that KDM3A and KDM4C are negatively correlated with stem cell aging in human.

DISCUSSION

Although heterochromatin reorganization is observed during cellular senescence, the physiological function of this unique epigenetic change is still ill defined. In this study, we have unveiled that KDM3A and KDM4C regulate condensin-dependent heterochromatin reorganization to restrain DDR during MSC senescence. Deficiency of *Kdm3a* leads to accelerated MSC senescence and premature bone aging in mice. From a clinical perspective, reduced expression of *KDM3A/KDM4C* or condensin component genes *NCAPD2* and *NCAPG2* can be utilized as indicators for aging.

Significant chromatin structural changes occur during physiological aging and cellular senescence, which include global histone loss, alternation of epigenetic landscapes, loss of heterochromatic regions, and large-scale chromatin rearrangements(Corpet and Stucki, 2014; Dowen et al., 2013; Lopez-Otin et al., 2013; Murga et al., 2007). However, it is interesting to note that different senescence models may have disparate and unique chromatin changes. We have illustrated that MSC replicative senescence is accompanied by heterochromatin reorganization at the early stage and heterochromatin loss at the final stage. In particular, upon senescence entry, a spatial reorganization of heterochromatin structure is manifested by redistribution and condensation of heterochromatin from nuclear membrane to nucleoplasm (Figure 1C). The dynamic change of heterochromatin is also observed in DOX-induced senescence model, which displays a gradual heterochromatin reorganization followed by a rapid heterochromatin destruction after

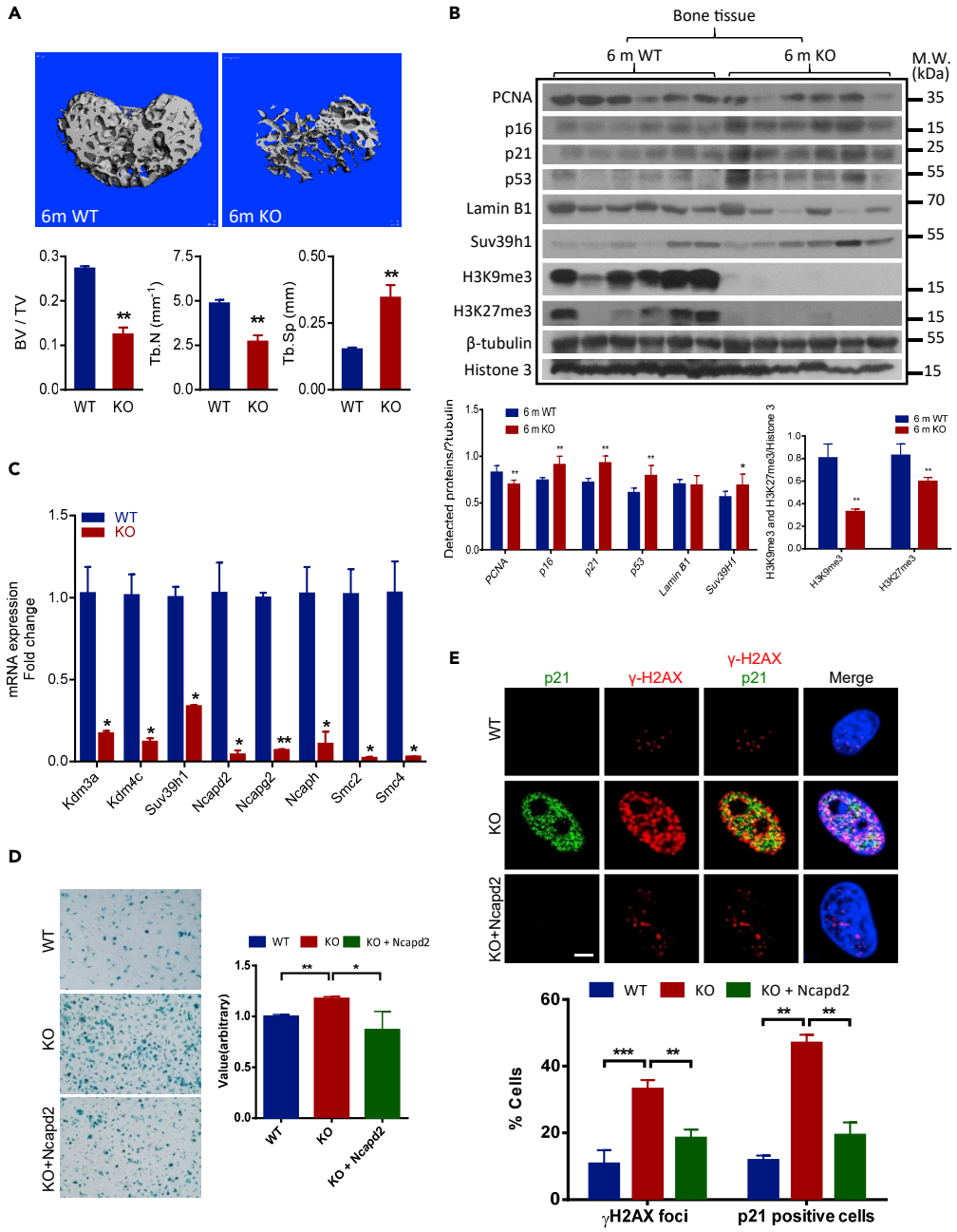

Figure 6. Deficiency of *Kdm3a* Leads to MSC Senescence and Bone Aging in Mice

(A) The representative three-dimensional reconstructed images of distal femur in a 6-month-old female *Kdm3a*$^{-/-}$ mice and WT mice by CT scanner. Quantification of morphometric parameters including bone volume fraction (BV/TV), trabecular number (Tb.N, 1/mm), and trabecular separation (Tb.Sp, mm) are shown at right. Data are presented as the mean ± SEM, **p < 0.01 (t test, n = 6).

(B) Western blot assay showing the expression of senescence markers p16, p21, p53, and heterochromatin markers H3K9me3 and H3K27me3 in bone tissues collected from 6-month-old *Kdm3a*$^{-/-}$ KO mice (n = 6) and WT mice (n = 6). Experiments were repeated three times, *p < 0.05; **p < 0.01 (Wilcoxon/Mann-Whitney test).

(C) RT-qPCR assay showing the reduction of condensin components in bone tissues collected from 6-month-old *Kdm3a*$^{-/-}$ KO mice. Data are presented as the mean ± SEM, *p < 0.05; **p < 0.01 (t test, n = 3).

(D) Representative images and quantification of β-Gal staining (scale bar = 100μm) show Ncapd2 rescues Doxorubicin-induced cellular senescence in KO BMSCs. Quantification data represents mean ± SEM of values from three independent experiments with three pairs of WT and KO mMSCs. *p < 0.05; **p < 0.01 (t test, n = 3).

Figure 6. *Continued*

(E) Representative images and quantification of γ-H2A.X and p21 immunofluorescence staining (scale bar = 5μm). Overexpression of *ncapd2* in KO BMSCs completely rescues Doxorubicin-induced DNA damage and heterochromatin destruction. Quantification data are presented as mean ± SEM of values from three different experiments with three pairs of WT and KO mMSCs. In each experiment, cells were derived from triplicate wells and analyzed on 6–8 cells/field from five different fields. **p < 0.01; ***p < 0.001 (t test, n = 3).

genotoxic treatment (Figures 4A and 4B). In line with the cell models, the stage-dependent change of heterochromatin has been recapitulated in OVX-induced bone aging model, which demonstrates a dynamic change of heterochromatin marks in primary BMSCs collected at different time points along with disease progression (Figures 5A and 5B). Altogether, it is clear that a stage-dependent heterochromatin reorganization process exists in conjunction with MSC senescence, misregulation of which could be detrimental as heterochromatin perturbation has been observed in progeria syndrome (Goldman et al., 2004; Scaffidi and Misteli, 2006; Shumaker et al., 2006; Zhang et al., 2015), and heterochromatin disorganization was proposed to underlie the pathogenesis of premature MSC aging in Werner syndrome (Zhang et al., 2015).

Interestingly, we have found that KDM3A and KDM4C are concomitantly upregulated along with heterochromation process at the early stage of replicative and DNA damage–induced senescence (Figures 1D and 4A–4C). Knockdown or suppression of *KDM3A* and *KDM4C* downregulates chromosome organization genes, whereas overexpression of *KDM3A* and *KDM4C* induces them (Figures 3 and S4). Condensin complex is of paramount importance for chromosome assembly and compaction during mitosis and meiosis (Hagstrom et al., 2002; Mishima et al., 2002). However, recent studies provide evidence that condensin complex might be involved in other biological processes. Previous studies have illustrated that condensins shape chromatin organization by its localization to topologically associating domain (TAD) boundaries in *Drosophila,* mouse, and human embryonic stem cells, indicating their regulatory role in chromatin high order organization in diverse interphase processes(Bauer et al., 2012). In addition, condensin complex binds to promoters and enhancers and participates in gene regulation in a variety of organisms (Ono et al., 2003, 2013; Tanaka et al., 2012). Despite of all these links, the potential role of condensin complex in the heterochromatin organization and cellular senescence had not been investigated until one recent study showed that condensin complex II subunit NCAPH2 was increased in oncogene-induced cancer cell lines (Yokoyama et al., 2015). In addition, overexpression of *NCAPH2* was sufficient to induce the formation of SAHF, whereas knockdown of *NCAPH2* reduced oncogene-induced cellular senescence in IMR90 fibroblasts (Yokoyama et al., 2015). This study raises unresolved fundamental questions of how condensin complex is induced upon senescence entry and what is the functional role of condensin complex during physiological aging. In the current study, we have unveiled that KDM3A and KDM4C induce the expression of both condensin I and II complex components at the early stage of MSC senescence via the H3K9 demethylase activity (Figures 3B–3E). Condensin complex I subunit NCAPD2 and condensin complex II subunit NCAPG2 promote heterochromatin condensation and reorganization, and overexpression of the condensin complex subunit rescues DOX-induced cellular senescence and heterochromatin destruction in *Kdm3a* KO MSCs (Figures 6D, 6E, and S6). In addition, suppression of KDMs alleviates the recruitment of condensin on the repetitive DNA sequences (Figure 3F). Positive correlation between *KDM3A/KDM4C* and condensin components has been demonstrated in *Kdm3a* KO mice and human stem cells, which are associated with aging (Figures 6C and 7). Altogether, these results suggest that condensin complex mediates the regulatory role of KDM3A and KDM4C in heterochromatin reorganization after the initial growth arrest during cellular senescence.

Activation of DDR is thought to enforce cellular senescence by imposing permanent checkpoints (d'Adda di Fagagna, 2008; d'Adda di Fagagna et al., 2003; Di Leonardo et al., 1994). Although DDR and chromatin reorganization have been both causally implicated in the establishment of cellular senescence, their relationship remains largely undefined (Liu et al., 2012; Mah et al., 2010; Sedelnikova et al., 2004). In our study, we observed that inhibition of KDM3A or KDM4C induced a striking DDR at the early stage of MSC senescence (Figure 2C). Because KDM3A and KDM4C is important for heterochromatin reorganization, we hypothesized that by hindering access of DNA damage sensors and associated DDR factors, heterochromatin can restrain DDR signaling in senescent stem cells, which functions as a protective machinery against senescence progression. To test this, we employed a genotoxic damage–induced cellular senescence model and clearly demonstrated that DOX induced a progressive heterochromatin reorganization process in advance of the activation of DDR (Figures 4A–4C). Suppression of *KDM3A* and *KDM4C* dramatically enhanced DOX-induced DDR signaling and cellular senescence (Figures 4D, S5A, and S5B), whereas overexpression of *KDM3A/KDM4C* or condensin component attenuated the DDR and senescence (Figures 4E and S5C), suggesting heterochromatin perturbation leads to an increase of DDR signaling in genotoxic damage–induced senescence. This assumption is further supported by the finding

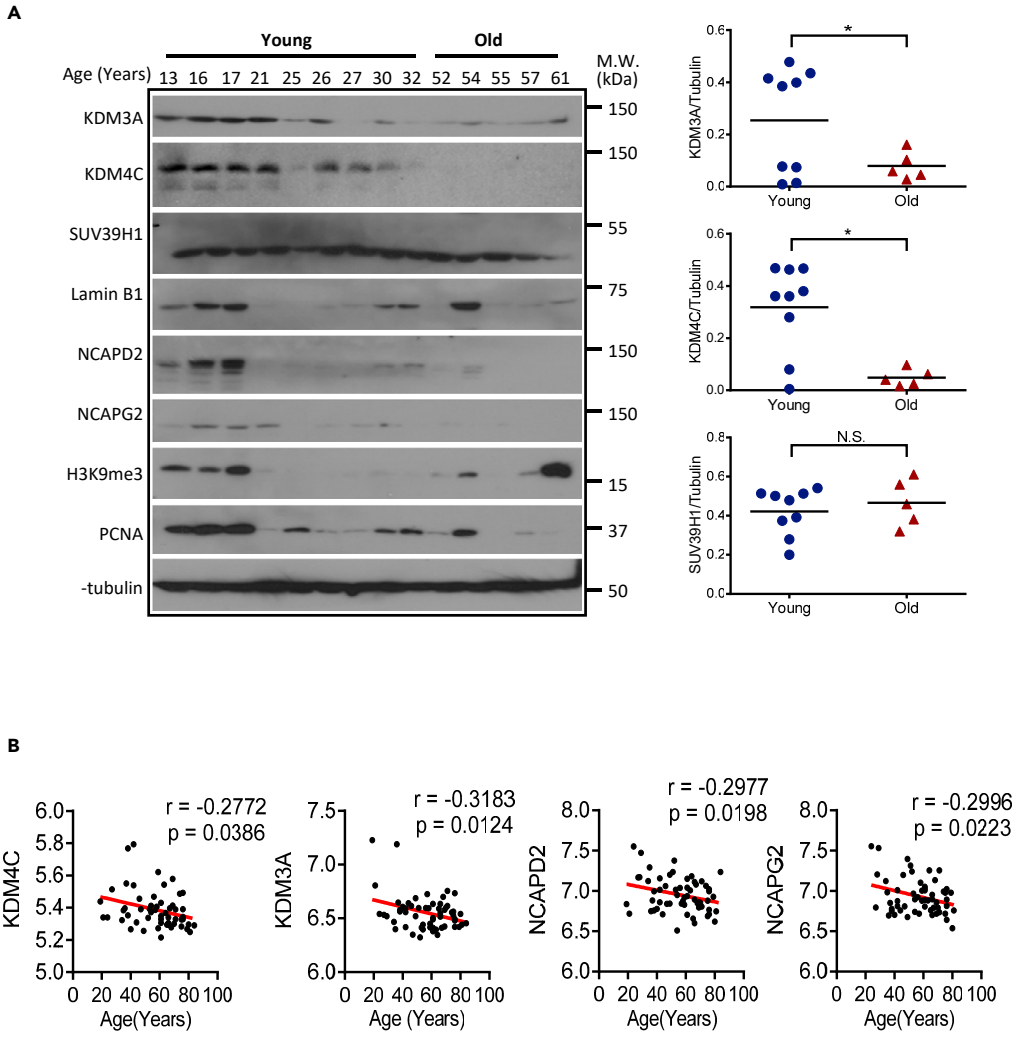

Figure 7. Expression Levels of *KDM3A/KDM4C and NCAPD2/NCAPG2* Are Inversely Correlated with Human Aging

(A) Western blot assay showing the expression levels of KDM3A, KDM4C, heterochromatin marks, and condensin components are globally reduced in old hBMSCs compared with young hBMSCs. Human bone marrow MSCs from 14 healthy individuals (Male, Asian, age range from 13 to 61 years) were cultured for three passages and used for further analysis. Quantification of KDM3A and KDM4C is shown at right. Data are presented as the mean ± SEM, *$p < 0.05$ (Wilcoxon/Mann-Whitney test).

(B) Negative correlations between *KDM3A*, *KDM4C*, *NCAPD2*, and *NCAPG2* (y axis) and age (x axis) in human MSCs samples (n = 60, age range from 19 to 84 years) (GEO: GSE39540).

that *Kdm3a* KO mice that exhibit a defective condensin machinery are more sensitive to DOX-induced DDR (Figures S7G and S7H). Heterochromatin has been reported to pose a barrier to DDR signaling (d'Adda di Fagagna, 2008; d'Adda di Fagagna et al., 2003; Di Micco et al., 2011; Murga et al., 2007). In *Drosophila*, HP1 prevents DDR activation at chromosome ends (Fanti et al., 1998), and in mammals it modulates DDR activation (Ayoub et al., 2009; Kim and Haber, 2009). Our results are consistent with a scenario in which heterochromatinization plays important role in restraining DDR signaling pathways, which can be achieved by both confining the access of DNA damage sensors to DNA lesions and impairing local signal amplification, thus blocking the augmentation of DNA damage and preventing senescence progression (Di Micco et al., 2011). Given the established role of condensin complex in higher-order genome organization, our results strongly suggest that KDM3A and KDM4C restrain accumulation of DNA damage via condensin-mediated heterochromatin organization during senescence progression.

Another important finding from this study is that both KDM3A/KDM4C and condensin components are inversely correlated with stem cell aging in humans. We have found that the expression levels of KDM3A and KDM4C dramatically decrease in old BMSCs compared with young BMSCs, which is accompanied by a marked reduction of heterochromatin marks and NCAPD2 and NCAPG2, supporting the transcriptional regulatory role of KDM3A and KDM4C in the condensin components and other chromosome condensation genes (Figure 7). The global reduction of KDM3A, KDM4C, and core chromosome organization genes demonstrated in DOX-induced senescence model (Figure 4A) is in accordance with the marked reduction of these genes observed in aging human BMSCs. Given the established link between DNA damage and human aging, it is explicable that along with human aging, hBMSCs gradually lose KDM3A- and KDM4C-mediated heterochromatin organization machinery, which adversely makes these stem cells more susceptible to genotoxic damage. Of note, although previous study using a Werner syndrome stem cell model showed that SUV39H1 is critical for maintaining the normal heterochromatin organization, loss of which led to deregulated heterochromatin structure (Zhang et al., 2015), we did not observe any significant change of SUV39H1 in old BMSCs compared with young BMSCs (Figure 7A). Thus, it appears that distinctive epigenetic regulatory mechanisms may underlie chronological and pathological aging process.

In summary, our study has revealed a role of histone demethylases in modulating heterochromatin reorganization, which functions as a defensive mechanism against DNA damage accumulation in stem cell senescence. As chemically modifiable enzymes, KDM3A and KDM4C could be activated or deactivated to regulate stem cell senescence, thereby holding promising potentials as therapeutic targets for intervening geriatric diseases and stem cell–mediated regenerative medicine. Additionally, in view of the importance of chromosome organization in a wide variety of biological processes, the presently demonstrated critical role of H3K9 demethylases provides insights into the molecular basis underlying other physiological or pathological conditions, such as embryonic development and cancer.

Limitations of the Study

We demonstrate that a panel of condensin components is regulated by KDM3A and/or KDM4C in MSC replicative senescence model and *Kdm3a* KO mouse model. Although our data show that the regulatory effect is attributed to the demethylase activity of KDM3A and KDM4C, we cannot exclude the possibility that other histone modifiers or transcription factors are involved in the regulatory process. Further work would also be required to definitively identify the relevant demethylase targets. Moreover, the current understanding of the link between heterochromatin reorganization and DDR in physiological condition is still elusive. Although we found that deficiency of *Kdm3a* disrupts heterochromatin reorganization and aggravates DDR during MSC senescence, additional experiments are needed to elucidate the underlying protective mechanism.

METHODS

All methods can be found in the accompanying Transparent Methods supplemental file.

SUPPLEMENTAL INFORMATION

Supplemental Information can be found online at https://doi.org/10.1016/j.isci.2019.10.041.

ACKNOWLEDGMENT

This work is supported by Hong Kong Food and Health Bureau (01120056, 03140496), and UGC/GRF, Hong Kong (14119516, 14165217, 14111519). The work is also supported by National Natural Science Foundation of China (NSFC No. 31771517), China and Guang Dong Province Science and Technology Grant (2017A050506043).

AUTHOR CONTRIBUTIONS

Biao Huang: experimental design and preformation, collection and/or assembly of data, data analysis, interpretation, and manuscript writing.

Bin Wang: experimental preformation, collection and/or assembly of data, data analysis, and interpretation.

Wayne Yuk-Wai Lee, Kin Pong U, and Kam Tong Leung: isolation and collection of human bone marrow MSCs.

Liu Shi, Lai Ling Tsang, Jiacheng Lin, Hailong Liu, and Xican Li: conduction of *in vivo* experiment, collection and/or assembly of *in vivo* data, data analysis, and interpretation.

Zhenqing Liu: collection and/or assembly of *in vitro* data, data analysis, and interpretation.

Rui Chen: CHIP-seq analysis.

Baohua Liu: generation of progeria mice and sample provision.

Yechun Ruan: discussion and interpretation of the data.

Hsiao Chang Chan: provision of study material, data analysis, and interpretation.

Gang Li: provision of study material, financial support, and technical support.

Xiaohua Jiang: conception and experimental design, financial support, provision of study material, data analysis and interpretation, and manuscript writing.

DECLARATION OF INTERESTS

The authors declare no competing interests.

Received: April 11, 2019
Revised: August 30, 2019
Accepted: October 21, 2019
Published: November 22, 2019

REFERENCES

Ayoub, N., Jeyasekharan, A.D., and Venkitaraman, A.R. (2009). Mobilization and recruitment of HP1: a bimodal response to DNA breakage. Cell Cycle *8*, 2945–2950.

Baker, N., Boyette, L.B., and Tuan, R.S. (2015). Characterization of bone marrow-derived mesenchymal stem cells in aging. Bone *70*, 37–47.

Bauer, C.R., Hartl, T.A., and Bosco, G. (2012). Condensin II promotes the formation of chromosome territories by inducing axial compaction of polyploid interphase chromosomes. PLoS Genet. *8*, e1002873.

Benayoun, B.A., Pollina, E.A., and Brunet, A. (2015). Epigenetic regulation of ageing: linking environmental inputs to genomic stability. Nat. Rev. Mol. Cell Biol. *16*, 593–610.

Boyette, L.B., and Tuan, R.S. (2014). Adult stem cells and diseases of aging. J. Clin. Med. *3*, 88–134.

Braig, M., Lee, S., Loddenkemper, C., Rudolph, C., Peters, A.H., Schlegelberger, B., Stein, H., Dorken, B., Jenuwein, T., and Schmitt, C.A. (2005). Oncogene-induced senescence as an initial barrier in lymphoma development. Nature *436*, 660–665.

Bulut-Karslioglu, A., De La Rosa-Velazquez, I.A., Ramirez, F., Barenboim, M., Onishi-Seebacher, M., Arand, J., Galan, C., Winter, G.E., Engist, B., Gerle, B., et al. (2014). Suv39h-dependent H3K9me3 marks intact retrotransposons and silences LINE elements in mouse embryonic stem cells. Mol. Cell *55*, 277–290.

Bustos, M.L., Huleihel, L., Kapetanaki, M.G., Lino-Cardenas, C.L., Mroz, L., Ellis, B.M., McVerry, B.J., Richards, T.J., Kaminski, N., Cerdenes, N., et al. (2014). Aging mesenchymal stem cells fail to protect because of impaired migration and antiinflammatory response. Am. J. Respir. Crit. Care Med. *189*, 787–798.

Caplan, A.I. (2005). Review: mesenchymal stem cells: cell-based reconstructive therapy in orthopedics. Tissue Eng. *11*, 1198–1211.

Chandra, T., Ewels, P.A., Schoenfelder, S., Furlan-Magaril, M., Wingett, S.W., Kirschner, K., Thuret, J.Y., Andrews, S., Fraser, P., and Reik, W. (2015). Global reorganization of the nuclear landscape in senescent cells. Cell Rep. *10*, 471–483.

Chandra, T., and Kirschner, K. (2016). Chromosome organisation during ageing and senescence. Curr. Opin. Cell Biol. *40*, 161–167.

Chandra, T., and Narita, M. (2013). High-order chromatin structure and the epigenome in SAHFs. Nucleus *4*, 23–28.

Chen, J.Y., Mou, X.Z., Du, X.C., and Xiang, C. (2015). Comparative analysis of biological characteristics of adult mesenchymal stem cells with different tissue origins. Asian Pac. J. Trop. Med. *8*, 739–746.

Collinson, A., Collier, A.J., Morgan, N.P., Sienerth, A.R., Chandra, T., Andrews, S., and Rugg-Gunn, P.J. (2016). Deletion of the polycomb-group protein EZH2 leads to compromised self-renewal and differentiation defects in human embryonic stem cells. Cell Rep. *17*, 2700–2714.

Corpet, A., and Stucki, M. (2014). Chromatin maintenance and dynamics in senescence: a spotlight on SAHF formation and the epigenome of senescent cells. Chromosoma *123*, 423–436.

d'Adda di Fagagna, F. (2008). Living on a break: cellular senescence as a DNA-damage response. Nat. Rev. Cancer *8*, 512–522.

d'Adda di Fagagna, F., Reaper, P.M., Clay-Farrace, L., Fiegler, H., Carr, P., Von Zglinicki, T., Saretzki, G., Carter, N.P., and Jackson, S.P. (2003). A DNA damage checkpoint response in telomere-initiated senescence. Nature *426*, 194–198.

Di Leonardo, A., Linke, S.P., Clarkin, K., and Wahl, G.M. (1994). DNA damage triggers a prolonged p53-dependent G1 arrest and long-term induction of Cip1 in normal human fibroblasts. Genes Dev. *8*, 2540–2551.

Di Micco, R., Sulli, G., Dobreva, M., Liontos, M., Botrugno, O.A., Gargiulo, G., dal Zuffo, R., Matti, V., d'Ario, G., Montani, E., et al. (2011). Interplay between oncogene-induced DNA damage

response and heterochromatin in senescence and cancer. Nat. Cell Biol. *13*, 292–302.

Dowen, J.M., Bilodeau, S., Orlando, D.A., Hubner, M.R., Abraham, B.J., Spector, D.L., and Young, R.A. (2013). Multiple structural maintenance of chromosome complexes at transcriptional regulatory elements. Stem Cell Reports *1*, 371–378.

Fanti, L., Dorer, D.R., Berloco, M., Henikoff, S., and Pimpinelli, S. (1998). Heterochromatin protein 1 binds transgene arrays. Chromosoma *107*, 286–292.

Gharibi, B., Farzadi, S., Ghuman, M., and Hughes, F.J. (2014). Inhibition of Akt/mTOR attenuates age-related changes in mesenchymal stem cells. Stem Cells *32*, 2256–2266.

Goldman, R.D., Shumaker, D.K., Erdos, M.R., Eriksson, M., Goldman, A.E., Gordon, L.B., Gruenbaum, Y., Khuon, S., Mendez, M., Varga, R., et al. (2004). Accumulation of mutant lamin A causes progressive changes in nuclear architecture in Hutchinson-Gilford progeria syndrome. Proc. Natl. Acad. Sci. U S A *101*, 8963–8968.

Hagstrom, K.A., Holmes, V.F., Cozzarelli, N.R., and Meyer, B.J. (2002). C. elegans condensin promotes mitotic chromosome architecture, centromere organization, and sister chromatid segregation during mitosis and meiosis. Genes Dev. *16*, 729–742.

Hebbar, M., Chandra, T., Shukla, A., Kadavigere, R., and Girisha, K.M. (2017). Complexities in genotype-phenotype correlation and genetic counseling in collagen VI - related myopathy. Indian J. Pediatr. *84*, 330–331.

Johmura, Y., Sun, J., Kitagawa, K., Nakanishi, K., Kuno, T., Naiki-Ito, A., Sawada, Y., Miyamoto, T., Okabe, A., Aburatani, H., et al. (2016). SCF(Fbxo22)-KDM4A targets methylated p53 for degradation and regulates senescence. Nat. Commun. *7*, 10574.

Kim, J.A., and Haber, J.E. (2009). Chromatin assembly factors Asf1 and CAF-1 have overlapping roles in deactivating the DNA damage checkpoint when DNA repair is complete. Proc. Natl. Acad. Sci. U S A *106*, 1151–1156.

Kuroki, S., Matoba, S., Akiyoshi, M., Matsumura, Y., Miyachi, H., Mise, N., Abe, K., Ogura, A., Wilhelm, D., Koopman, P., et al. (2013). Epigenetic regulation of mouse sex determination by the histone demethylase Jmjd1a. Science *341*, 1106–1109.

Lin, S.P., Chiu, F.Y., Wang, Y., Yen, M.L., Kao, S.Y., and Hung, S.C. (2014). RB maintains quiescence and prevents premature senescence through upregulation of DNMT1 in mesenchymal stromal cells. Stem Cell Reports *3*, 975–986.

Liu, B., Yip, R., and Zhou, Z. (2012). Chromatin remodeling, DNA damage repair and aging. Curr. Genomics *13*, 533–547.

Liu, Z., Zhou, S., Liao, L., Chen, X., Meistrich, M., and Xu, J. (2010). Jmjd1a demethylase-regulated histone modification is essential for cAMP-response element modulator-regulated gene expression and spermatogenesis. J. Biol. Chem. *285*, 2758–2770.

Lopez-Otin, C., Blasco, M.A., Partridge, L., Serrano, M., and Kroemer, G. (2013). The hallmarks of aging. Cell *153*, 1194–1217.

Mah, L.J., El-Osta, A., and Karagiannis, T.C. (2010). gammaH2AX: a sensitive molecular marker of DNA damage and repair. Leukemia *24*, 679–686.

Mani, P., Keshavarz, T., Chandra, T.S., and Kyazze, G. (2017). Decolourisation of Acid orange 7 in a microbial fuel cell with a laccase-based biocathode: influence of mitigating pH changes in the cathode chamber. Enzyme Microb. Technol. *96*, 170–176.

Merkwirth, C., Jovaisaite, V., Durieux, J., Matilainen, O., Jordan, S.D., Quiros, P.M., Steffen, K.K., Williams, E.G., Mouchiroud, L., Tronnes, S.U., et al. (2016). Two conserved histone demethylases regulate mitochondrial stress-induced longevity. Cell *165*, 1209–1223.

Mishima, M., Kaitna, S., and Glotzer, M. (2002). Central spindle assembly and cytokinesis require a kinesin-like protein/RhoGAP complex with microtubule bundling activity. Dev. Cell *2*, 41–54.

Mosammaparast, N., and Shi, Y. (2010). Reversal of histone methylation: biochemical and molecular mechanisms of histone demethylases. Annu. Rev. Biochem. *79*, 155–179.

Munoz-Espin, D., and Serrano, M. (2014). Cellular senescence: from physiology to pathology. Nat. Rev. Mol. Cell Biol. *15*, 482–496.

Murga, M., Jaco, I., Fan, Y., Soria, R., Martinez-Pastor, B., Cuadrado, M., Yang, S.M., Blasco, M.A., Skoultchi, A.I., and Fernandez-Capetillo, O. (2007). Global chromatin compaction limits the strength of the DNA damage response. J. Cell Biol. *178*, 1101–1108.

Narita, M., Nunez, S., Heard, E., Narita, M., Lin, A.W., Hearn, S.A., Spector, D.L., Hannon, G.J., and Lowe, S.W. (2003). Rb-mediated heterochromatin formation and silencing of E2F target genes during cellular senescence. Cell *113*, 703–716.

Ono, T., Losada, A., Hirano, M., Myers, M.P., Neuwald, A.F., and Hirano, T. (2003). Differential contributions of condensin I and condensin II to mitotic chromosome architecture in vertebrate cells. Cell *115*, 109–121.

Ono, T., Yamashita, D., and Hirano, T. (2013). Condensin II initiates sister chromatid resolution during S phase. J. Cell Biol. *200*, 429–441.

Patel, H., Mayl, J., Chandra, B., Pritchett, C., and Chandra, T. (2016). Dermoid of the oral cavity: case report with histopathology correlation and review of literature. J. Radiol. Case Rep. *10*, 19–27.

Peters, A.H., O'Carroll, D., Scherthan, H., Mechtler, K., Sauer, S., Schofer, C., Weipoltshammer, K., Pagani, M., Lachner, M., Kohlmaier, A., et al. (2001). Loss of the Suv39h histone methyltransferases impairs mammalian heterochromatin and genome stability. Cell *107*, 323–337.

Scaffidi, P., and Misteli, T. (2006). Lamin A-dependent nuclear defects in human aging. Science *312*, 1059–1063.

Sedelnikova, O.A., Horikawa, I., Zimonjic, D.B., Popescu, N.C., Bonner, W.M., and Barrett, J.C. (2004). Senescing human cells and ageing mice accumulate DNA lesions with unrepairable double-strand breaks. Nat. Cell Biol. *6*, 168–170.

Sen, P., Dang, W., Donahue, G., Dai, J., Dorsey, J., Cao, X., Liu, W., Cao, K., Perry, R., Lee, J.Y., et al. (2015). H3K36 methylation promotes longevity by enhancing transcriptional fidelity. Genes Dev. *29*, 1362–1376.

Shumaker, D.K., Dechat, T., Kohlmaier, A., Adam, S.A., Bozovsky, M.R., Erdos, M.R., Eriksson, M., Goldman, A.E., Khuon, S., Collins, F.S., et al. (2006). Mutant nuclear lamin A leads to progressive alterations of epigenetic control in premature aging. Proc. Natl. Acad. Sci. U S A *103*, 8703–8708.

Tanaka, A., Tanizawa, H., Sriswasdi, S., Iwasaki, O., Chatterjee, A.G., Speicher, D.W., Levin, H.L., Noguchi, E., and Noma, K. (2012). Epigenetic regulation of condensin-mediated genome organization during the cell cycle and upon DNA damage through histone H3 lysine 56 acetylation. Mol. Cell *48*, 532–546.

Tateishi, K., Miura, Y., Hayashi, S., Takahashi, M., and Kurosaka, M. (2009). DcR3 protects THP-1 macrophages from apoptosis by increasing integrin alpha4. Biochem. Biophys. Res. Commun. *389*, 593–598.

Turinetto, V., Vitale, E., and Giachino, C. (2016). Senescence in human mesenchymal stem cells: functional changes and implications in stem cell-based therapy. Int. J. Mol. Sci. *17*, 1164–1182.

Ugarte, F., Sousae, R., Cinquin, B., Martin, E.W., Krietsch, J., Sanchez, G., Inman, M., Tsang, H., Warr, M., Passegue, E., et al. (2015). Progressive chromatin condensation and H3K9 methylation regulate the differentiation of embryonic and hematopoietic stem cells. Stem Cell Reports *5*, 728–740.

Wilson, A., Shehadeh, L.A., Yu, H., and Webster, K.A. (2010). Age-related molecular genetic changes of murine bone marrow mesenchymal stem cells. BMC Genomics *11*, 229.

Wong, T.Y., Solis, M.A., Chen, Y.H., and Huang, L.L. (2015). Molecular mechanism of extrinsic factors affecting anti-aging of stem cells. World J. Stem Cells *7*, 512–520.

Yokoyama, Y., Zhu, H., Zhang, R., and Noma, K. (2015). A novel role for the condensin II complex in cellular senescence. Cell Cycle *14*, 2160–2170.

Yu, K.R., and Kang, K.S. (2013). Aging-related genes in mesenchymal stem cells: a mini-review. Gerontology *59*, 557–563.

Zhang, W., Li, J., Suzuki, K., Qu, J., Wang, P., Zhou, J., Liu, X., Ren, R., Xu, X., Ocampo, A., et al. (2015). Aging stem cells. A Werner syndrome stem cell model unveils heterochromatin alterations as a driver of human aging. Science *348*, 1160–1163.

Zhu, J., Adli, M., Zou, J.Y., Verstappen, G., Coyne, M., Zhang, X., Durham, T., Miri, M., Deshpande, V., De Jager, P.L., et al. (2013). Genome-wide chromatin state transitions associated with developmental and environmental cues. Cell *152*, 642–654.

ISCI, Volume *21*

Supplemental Information

KDM3A and KDM4C Regulate Mesenchymal Stromal Cell Senescence and Bone Aging via Condensin-mediated Heterochromatin Reorganization

Biao Huang, Bin Wang, Wayne Yuk-Wai Lee, Kin Pong U, Kam Tong Leung, Xican Li, Zhenqing Liu, Rui Chen, Jia cheng Lin, Lai Ling Tsang, Baohua Liu, Ye chun Ruan, Hsiao Chang Chan, Gang Li, and Xiaohua Jiang

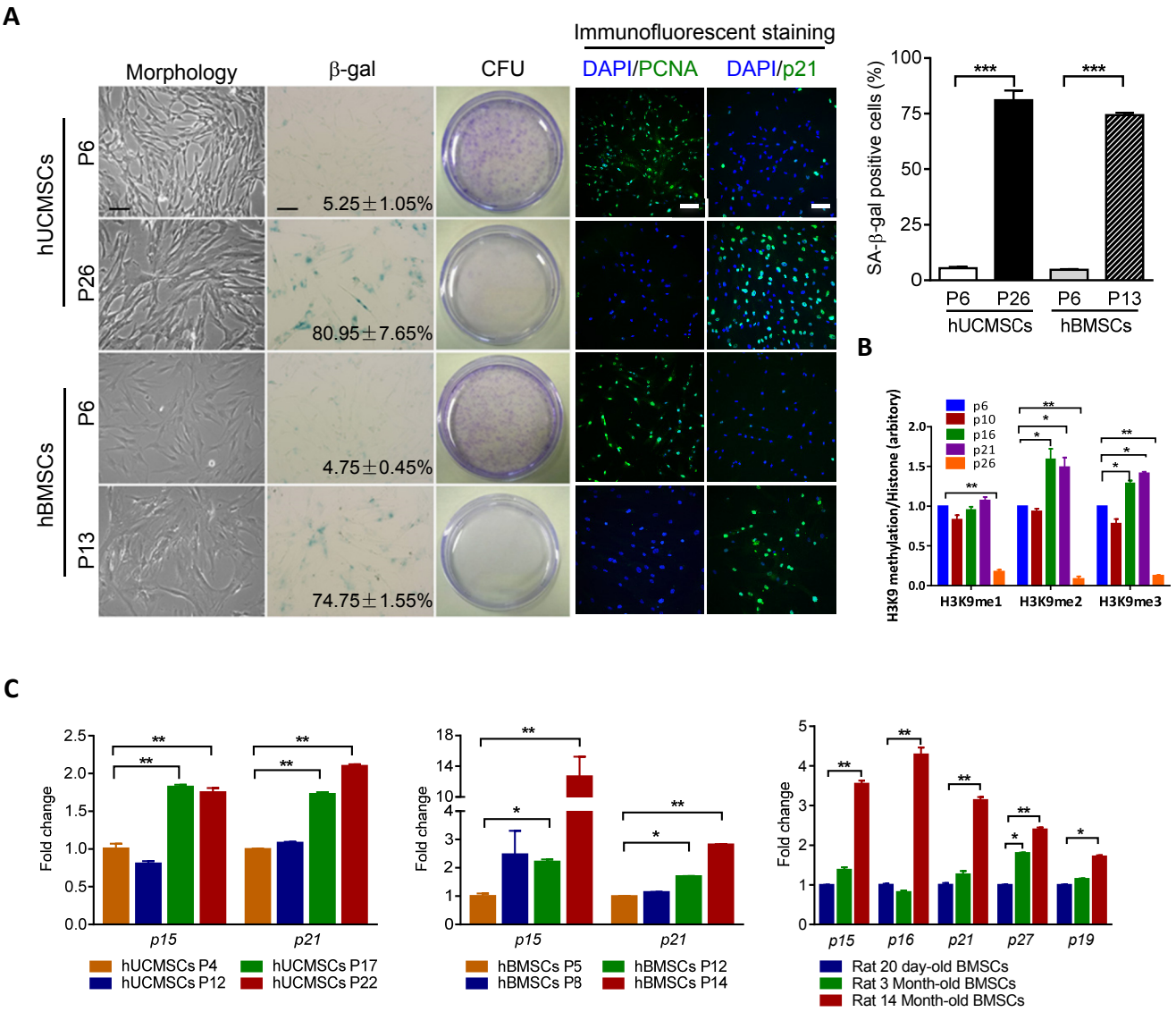

Supplementary Figure S1: Establishment of replicative senescence model using MSCs, Related to Figure 1

Three hUCMSCs lines (hUC009, hUC011, hUC013) and three hBMSCs lines (hBM001, hBM003, hBM005) were used for serial passaging, and characterized with various senescence markers. **(A)** Representative images of morphology, β-Gal staining, colony formation and immunofluorescence staining of PCNA and p21 (scale bar=100μm) in early passage hUCMSCs (p6) and hBMSCs (p6) compared with late passage hMSCs (p26 for hUCMSCs, p13 for hBMSCs). Quantification of β-Gal staining in early passage hUCMSCs and hBMSCs compared with late passage hMSCs. Data are presented as the mean ± SEM. ***p<0.001 (t test, n=3). **(B)** Quantification of protein expression of H3K9me, H3K9me2, H3K9me3 during MSC senescence as shown in Figure 1B. *p<0.05; **p<0.01(t test, n=3). **(C)** RT-qRCR analysis of cell cycle inhibitors in 3 senescence models. Data are presented as mean ± SEM. *p<0.05; **p<0.01 (t test, n=3). For Rat BMSCs, MSCs were isolated from the bone marrow of SD rats at different ages, (20 days, n=3; 3 months, n=3; 14 months, n=3).

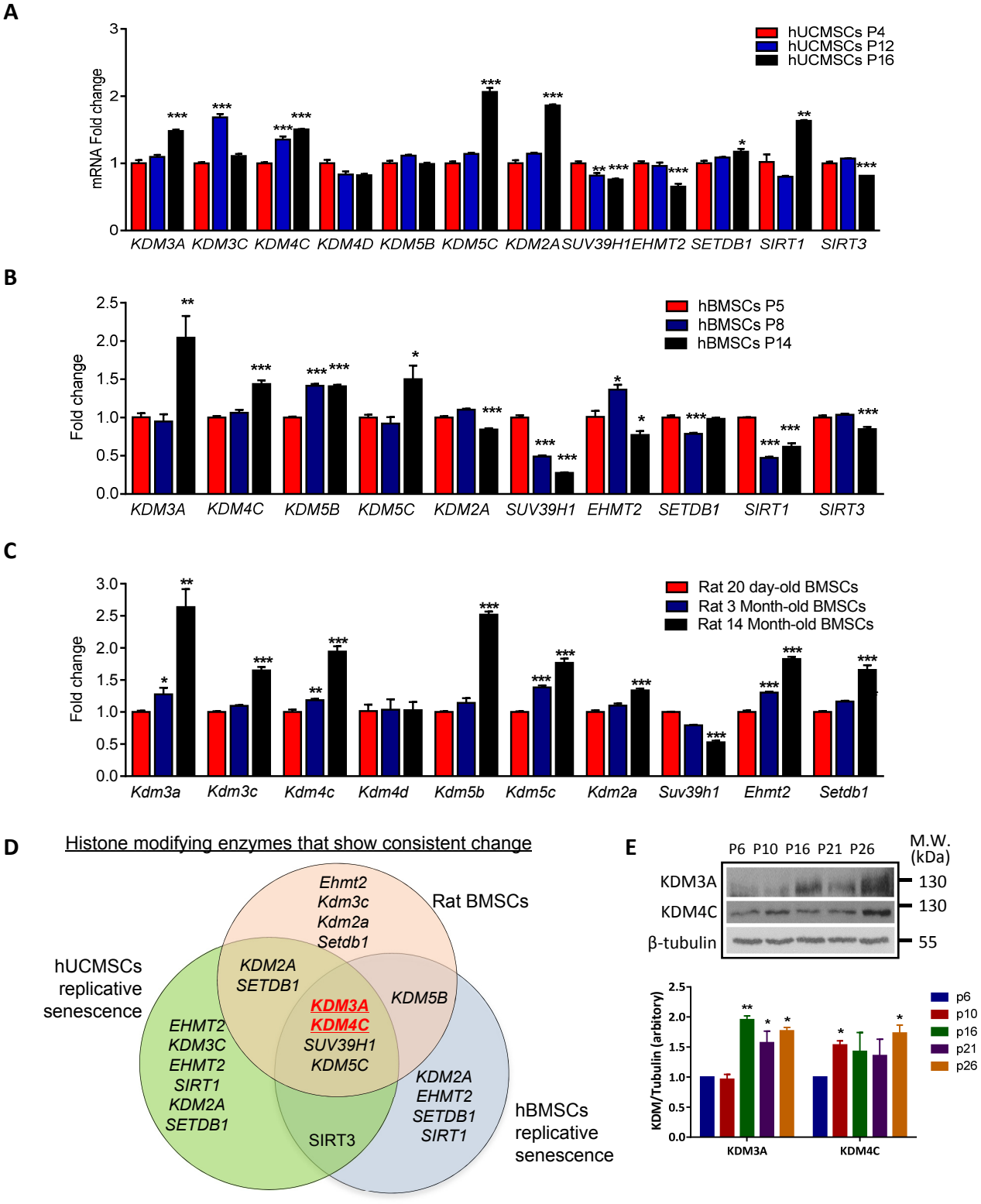

Supplementary Figure S2: Screening of histone-modifying enzymes involved in MSC senescence, Related to Figure 1
(A-C) Gene expression profiling of histone modifying enzymes in hUCMSCs replicative senescence model, hBMSCs replicative senescence model and primary rat BMSCs with physiological aging. Data are presented as the mean ± SEM. *p<0.05; **p<0.01;***p<0.001(t test n=3). **(D)** Venn diagram reveals the commonly differentially-expressed histone modifying enzymes in three senescence models. **(E)**Representative western blot showing the protein expression levels of KDM3A and KDM4C increase with hUCMSC aging. Experiments were repeated three times with two hUCMSCs lines, *p<0.05; **p<0.01 (t test, n=3).

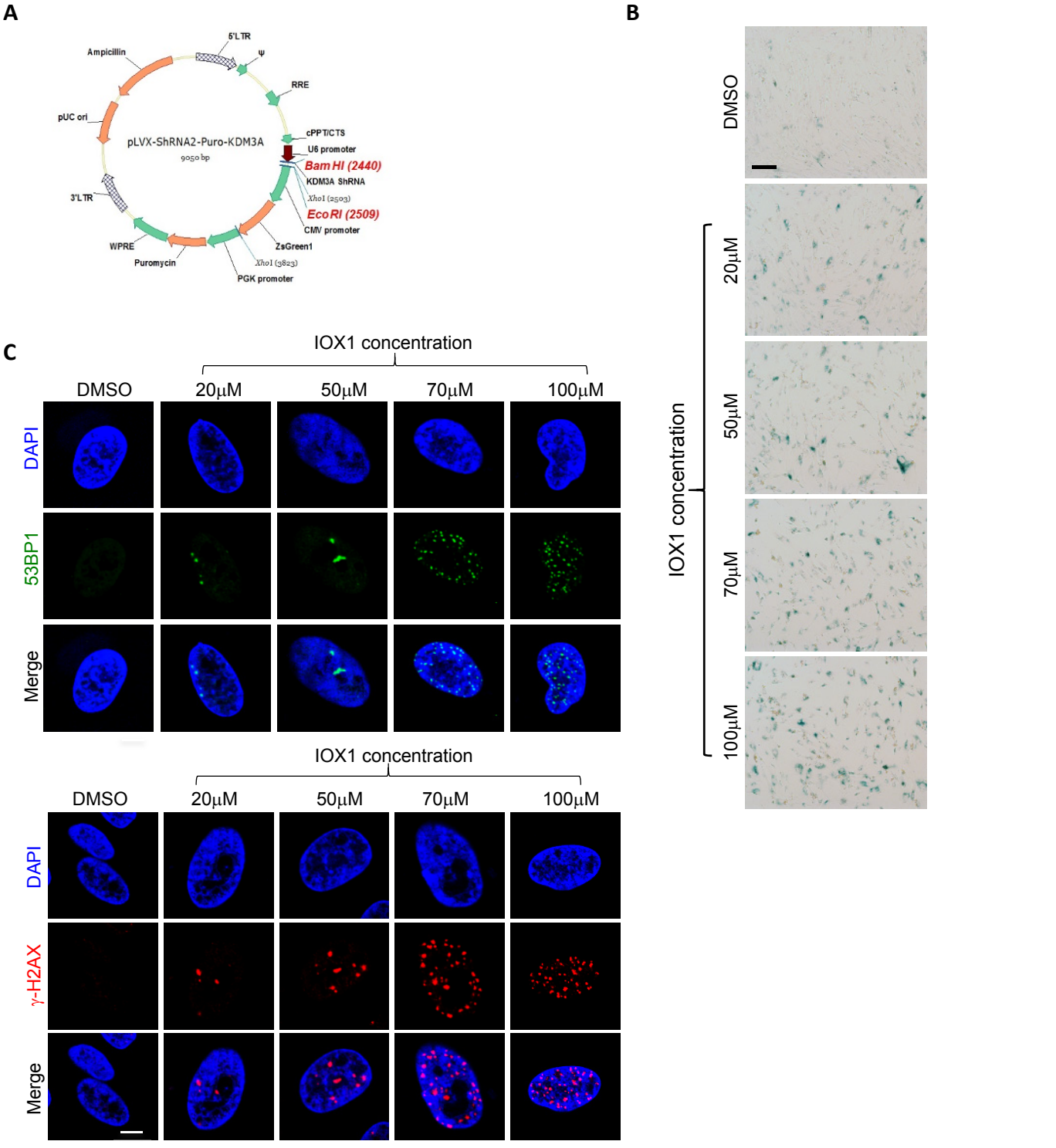

Supplementary Figure S3: KDM inhibitor IOX1 induces DNA damage and cellular senescence in MSCs, Related to Figure 2
(A) Map of lentiviral vector containing shRNA-KDM. **(B)** Representative images of β-Gal staining in hUCMSCs (p7) treated with different concentrations of IOX1 (scale bar=100μm). **(C)** Representative images of 53BP1 and γ-HA2X staining in hUCMSCs (p7) treated with different concentrations of IOX1 (scale bar=5μm).

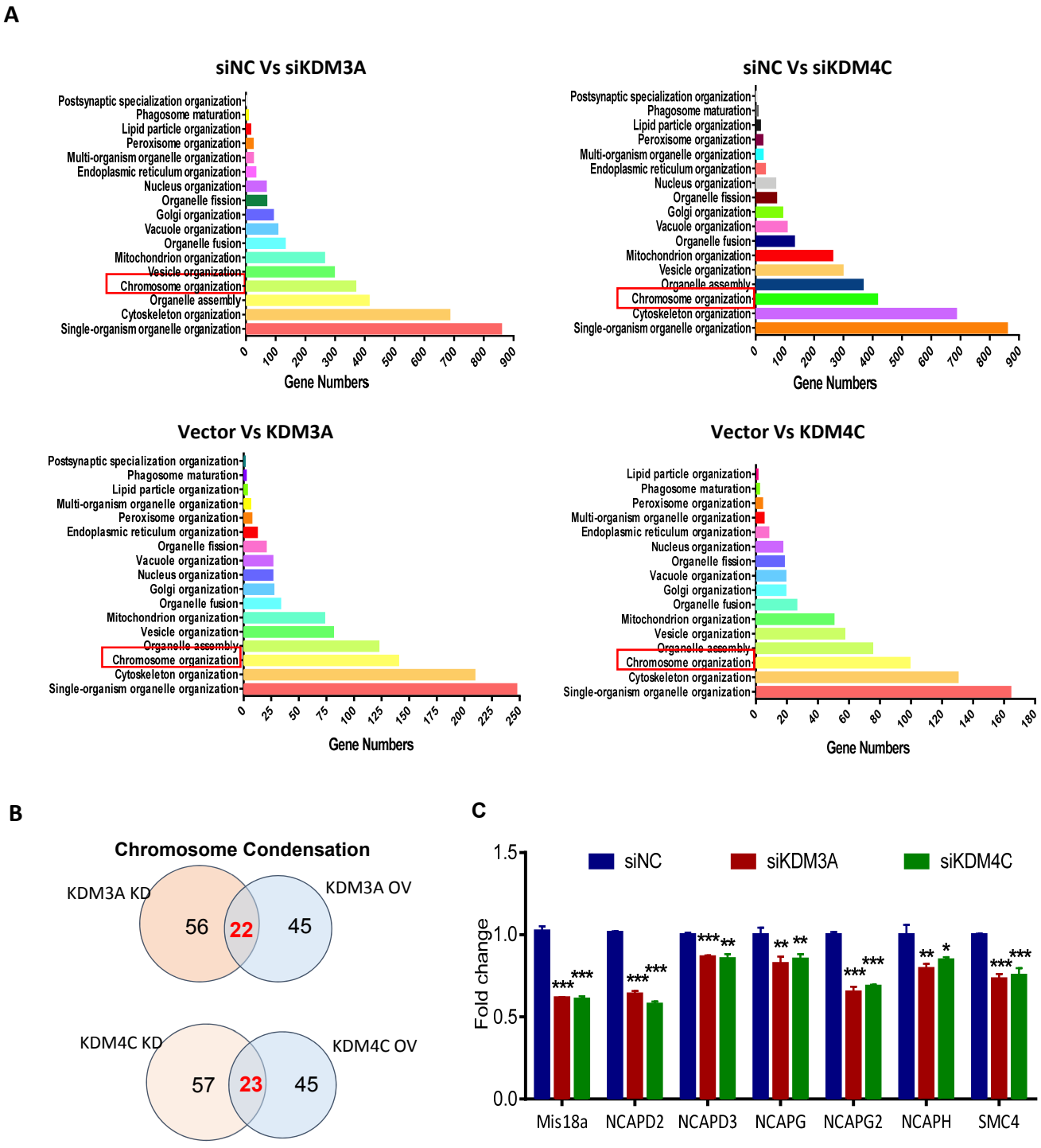

Supplementary Figure S4: KDM3A and KDM4C regulate chromosome condensation genes, Related to Figure 3
(A) GO analysis of differentially expressed genes (DEGs) on organelle organization based on RNA-Seq results comparing siKDM3A-1 or siKDM4C-3-treated hUCMSCs with Scrambled siRNA-treated hUCMSCs, or *KDM3A*- or *KDM4C*-overexpressing hUCMSCs with vector control-transfected hUCMSCs. **(B)** Venn diagram reveals the commonly differentially-expressed chromosome condensation genes in KD and overexpressing cells compared to their respective control cells. **(C)** RT-qPCR assay showing the expression levels of condensin subunits in siKDM3A-(siKDM3A-1+siKDM3A-3) or siKDM4C-(siKDM4C-1+siKDM4C-3) - or Scrambled siRNA-treated hUCMSCs. Data are presented as mean±SEM. *p<0.05; **p<0.01;***p<0.001 (test, n=3).

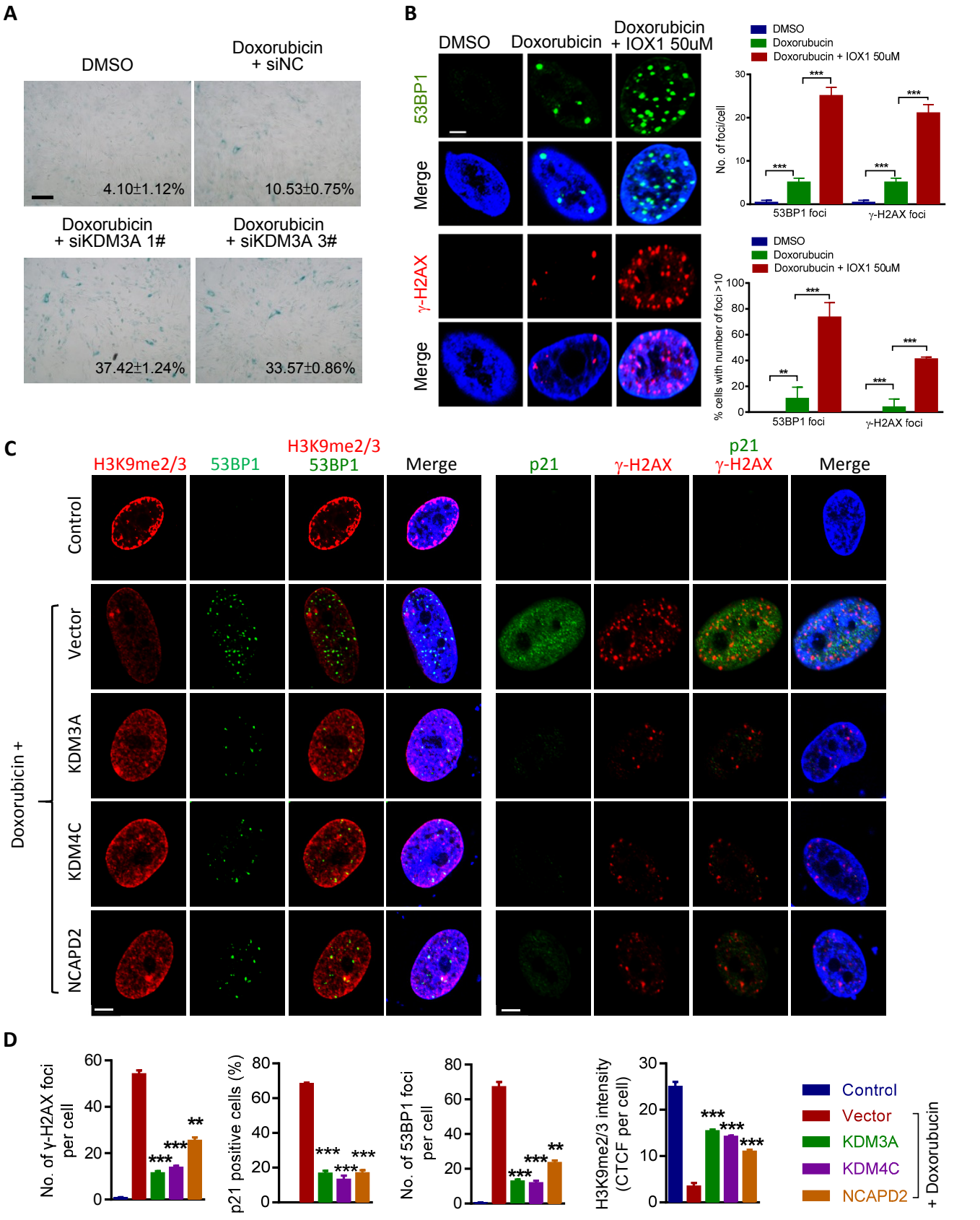

Supplementary Figure S5: KDM3A and KDM4C regulate DNA damage-induced senescence via NCAPD2, Related to Figure 4
(A) Representative images of β-Gal staining in Doxorubicin- treated hUCMSCs with Scrambled siRNAs or siKDM3A-1 or siKDM3A-3. (scale bar=100μm). **(B)** Representative images and quantification of 53BP1 and γ-H2AX immunofluorescence staining (scale bar=5μm) in hUCMSCs treated with Doxorubicin only or Doxorubicin + IOX1 50μM. mean±SEM of values from three different experiments with triplicate wells analyzed on 6-8 cells/field from five different fields ;***p<0.001 (t test). **(C-D)** Representative images and quantification of 53BP1, γ-H2AX, p21 and H3K9me2/3 immunofluorescence staining (scale bar=5μm) in control or Doxorubicin-treated hUCMSCs transfected with Vector plasmid or *KDM3A*, *KDM4C* or *NCAPD2* plasmid (CTCF, corrected total cell fluorescence). Mean±SEM of values from three different experiments with triplicate wells analyzed on 6-8 cells/field from five different fields. **p<0.01;***p<0.001 by t test compared to vector control treated with DOX.

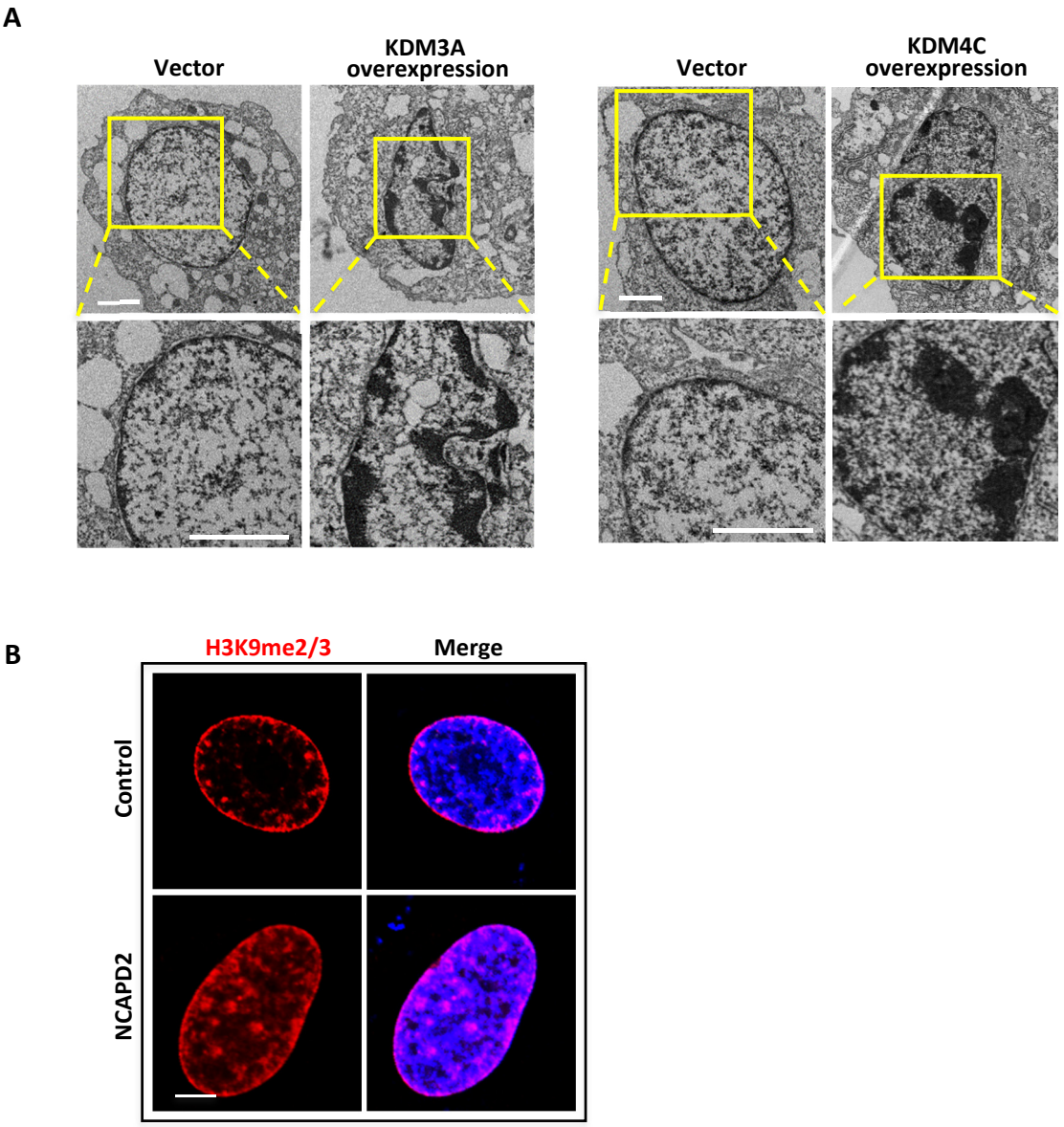

Supplementary Figure S6: KDM3A and KDM4C promote chromosome organization, Related to Figure 4
(A) Representative images of Transmission Electron Microscope (TEM) on the nucleus of hUCMSCs transfected with *KDM3A* or *KDM4C* or vector plasmid. The experiment was performed using hUC013. **(B)** Representative images showing overexpression of *NCAPD2* promotes formation of heterochromatin foci as demonstrated by H3K9me3 (red) staining (scale bar=5μm).

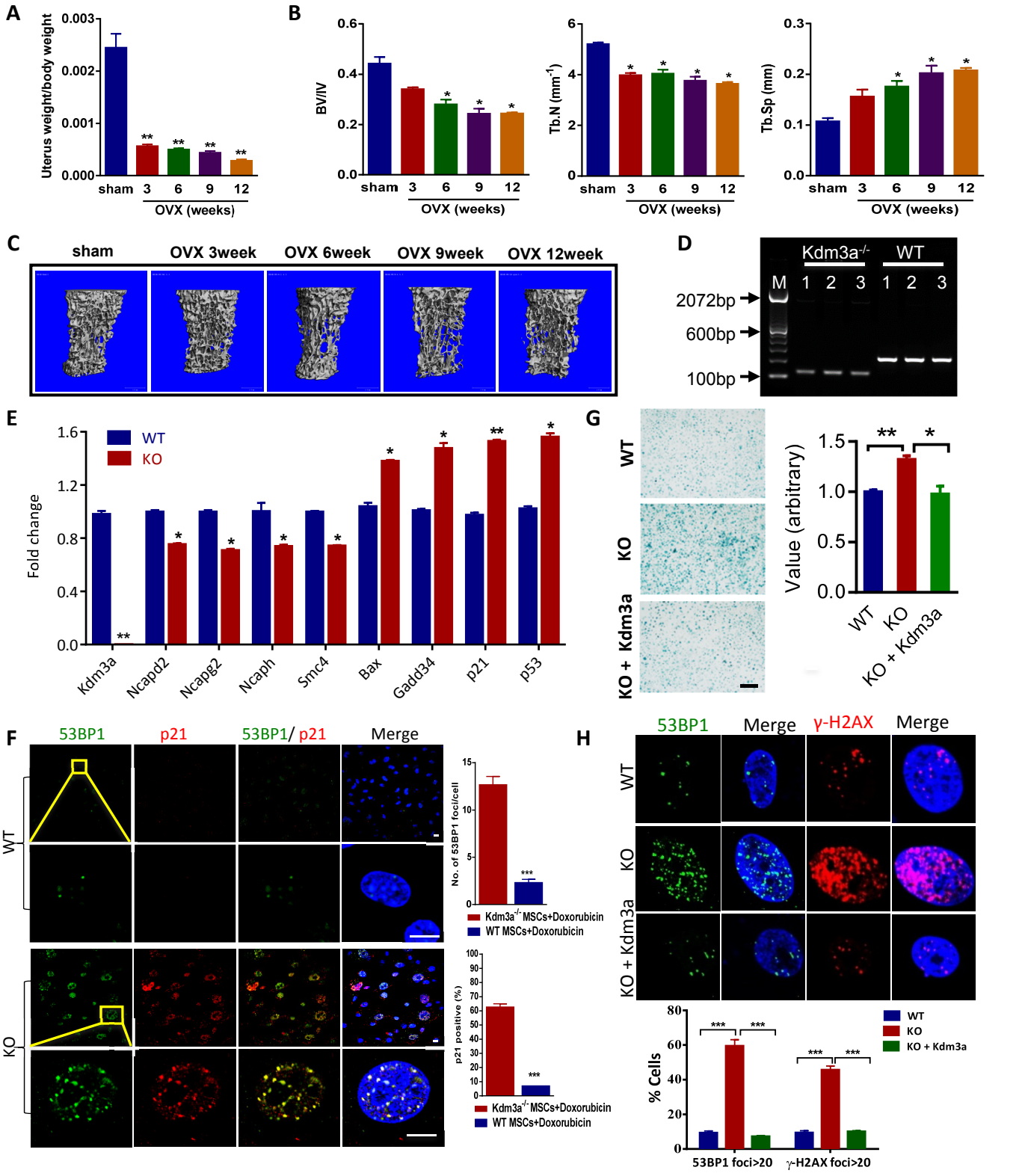

Supplementary Figure S7: Kdm3a affects bone aging *in vivo*, Related to Figure 5 and Figure 6

(A) Quantification data of uterus of sham and OVX-treated rats at 12 weeks (total n=29, sham group n=5, OVX 3weeks n=6, OVX 6weeks n=6, OVX 9weeks n=6, OVX 12weeks n=6). **p<0.01, (Wilcoxon/Mann-Whitney test). **(B)** The quantification of morphometric parameters including bone volume fraction (BV/TV), trabecular number (Tb.N, 1/mm) and trabecular separation (Tb.Sp, mm) in rat OVX rats. *p<0.05(Wilcoxon/Mann-Whitney test). **(C)** The representative three-dimensional reconstructed images of trabecular microarchitecture of 5th vertebral bodies in rat OVX rats. **(D)** Genotyping of WT and *Kdm3a* KO mice. **(E)** qPCR assay showing the downregulation of condensin components and upregulation of cell cycle regulators in BMSCs collected from 6 month-old *Kdm3a*$^{-/-}$ mice (n=3) compared to WT mice (n=3), *p<0.05;**p<0.01 (t test). **(F)** Representative images of immunofluorescence staining of p21 and 53BP1 in Doxorubicin (5 x 10^{-8} M)-treated BMSCs derived from 6 month-old *Kdm3a*$^{-/-}$ mice (n=3) and WT mice (n=3). Mean±SEM of values from three different experiments with triplicate wells analyzed on 6-8 cells/field from five different fields; ***p<0.001 (t test). **(G)** Representative images and quantification of β-Gal staining (scale bar=100μm) show KDM3A rescues Doxorubicin-induced cellular senescence in KO BMSCs. Each plate represents BMSCs derived from a single mouse, n=3 for each group. *p<0.05; **p<0.01 (t test). **(H)** Representative images and quantification of 53BP1 and γ-H2A.X immunofluorescence staining (scale bar=5μm). Overexpression of kdm3a in KO BMSCs completely rescues Doxorubicin-induced DNA damage (n=3). Data are presented as mean±SEM of values from three different experiments with triplicate wells analyzed on 6-8 cells/field from five different fields,***p<0.001 (t test).

Supplementary Table S1: Detailed information of BMSCs, Related to Figure 7

Inventory ID	Disease	Age	Gender	Race
BMMSC4 2009	Mild anemia	13	M	Asian
BMMSC5 2010	None	16	M	Asian
BMMSC7 2009	Mild anemia	17	M	Asian
BMMSC3 2009	None	21	M	Asian
BMMSCS04	None	26	M	Asian
BMMSCS01	None	27	M	Asian
BMMSCS006	None	30	M	Asian
BMMSCS05	None	32	M	Asian
BMMSCK009	None	25	M	Asian
BMMSCS005	None	61	M	Asian
BMMSC S007	None	52	M	Asian
BMMSC K006	None	55	M	Asian
BMMSC K005	None	54	M	Asian
BMMSC K008	None	57	M	Asian

Supplementary Table S2. Primers used in this study, Related to Figure 2, Figure 3, Figure 5 and Figure 6

Primers for qPCR (Human primers)

Target	Forward primer (5' to 3')	Reverse primer (5' to 3')
hKDM5A	TATCCCAAGCGACTACCCAC	TCCTGGATCTGTATGCTTTGA
hKDM5B	AGTTTGGGCCTCCAATTCAT	CGAGCAGACTGGCATCTGTA
hKDM5C	TTGTAGCCTTGGTTGAAGCC	ACCCTCATGAATCCCAACAC
hSIRT1	AGAGATGGCTGGAATTGTCC	CCAGATCCTCAAGCGATGTT
hSIRT3	AGAACACAATGTCGGGCTTC	CACAGTCTGCCAAAGACCCT
hEHMT2	GAGGTCACCTTTCCCAGTGA	AACCATGTCCAAACCAGGAA
hSETDB1	TTCACGGAGCTTCTGGTCTT	TTCCCGGCCTACAGAAATAA
hSUV39H1	ACACGTCCTCCACGTAGTCC	CAAGAACAGCTTCGTCATGG
hKDM4A	GGAGCTTGCTTAAAGGCTGA	GAAGCGCCGCTAGAAGTTT
hKDM4B	CGTCCATGGAGATCTTGACC	TTCAATCACGGGTTCAACTG
hKDM4C	TCACCATGTCTTTCCTGCAA	TTCCCATATGGCTACCATGC
hKDM4D	CCACATACCAAGTTTTGGGC	GTGGAAAACCACGTTTGCTT
hKDM3A	TTCTTTTCCTCCAAGATTCCC	GGGACCATTCGAGCTGTTT
hJMJD1C	AGTAAACCACTGGGTGGCAG	AGCCTTGTTGTGGATTTCTGA
hKDM2A	CCATCATCTTCATAGCGTCG	AGCCCTGGAGTGGTTTCTTT
hKDM2B	AGCTCCTGCCGTTGTCC	TGGCCAAAGAAGACTCCAAA
hKDM6B	CGCTGCCTCACCCATATCC	ATCCGCGACCTCTGAACTCT
hLMNB1	TCTTTCGAATTCAGTGCTGC	AAGTGCAAGGCGGAACAC
hCENPA	GTCTCCGCCGACTGTGTT	CCTCTGCGGCGTGTCAT
hH2AFZ	CTTTCCGGAGTCCTTTCCAG	GTGGGTCCGATTAGCCTTTT
hNCAPD2	GGCAGCCTGAAAAGCTCTAA	CCCCAGAGGAGTTGTTGAAA
hNCAPG2	AAATTCTTCAGCCTTTGCCAT	GCTGGTTGGAGAGTTTTTGC
hHJURP	CAAACAGAGAGCAAGTGGGA	TCTTCACAGCCCAACTCAGA
hMis18a	CAAGATTGAGTGAGCACCCC	ATCCTGCTTCGCTGTGTTTC

Primers for qPCR (Rat primers)

Target	Forward primer	Reverse primer
rKdm3a	TTGCTCTGAGGTCTCTCCCA	GCAGTACAGCCAAGCAGGAT
rJmjd1c	TGC GCT GAC CTT CAA ACC AT	GTT CGG GCT TTA GGC TGT CT
rKdm4c	TGG AGA GTC CCC TAA ATC CCA	TTG GCA AGA CCT GCT CGA TG
rKdm4d	AGGCGCAAATAAGTACGGGG	CGGGTGCAGCAGAATCTCTT
rKdm5b	GCC ACC ATT CGC TTG TGA TG	TTA CAC GTG TTT GGG CCT CC

rKdm5c	GGT TCC TTG CTA CGC TCT CA	TAC ACT GCA CAA GGT TGG CT
rKdm2a	GGCATCCGGGAGTGGTTTCT	TACCACGCAATCTCTGGCTG
rSuv39h1	GGCGCCACCTACCTCTTTGA	CGTTGTACACCTGCAGGTTG
rEhmt2	GAGCCGCCGAGAGAGTTC	GGTGTCAGCCCCCTCATC
rSetdb1	TTTGCAAAGTACTCATCACCCA	TTGGATGACATTGCTAAAGGCT
rSirt1	TCAAGGCTGTTGGTTCCAGT	AAGGCGTCATCTTCAGAGTC
rSirt3	GGCACTACAGGCCCAATGTC	TCTCTCAAGCCCGTCGATGT
rNcapd2	AATTGTGGGCAAACTGCGTC	CAGAGGCTGTTGCCTTGAGA
rNcapg2	TGCTTGAGTGCTGCTGTGTA	TGTGGCCTTGAGATACGACG
rCenpa	GGCACTACACAGAAGACGGA	CACACCACGGCTGAATTTCC
rHjurp	AGTCTGGGGAGGAAAGCTGA	AAGCTTGTATCTGCACCGCT
r p15/INK4b	TCACCAGACCTGTGCATGAT	AGGCGTCACACACATCCAG
r p16/INK4a	ACCAAACGCCCCGAACA	GAGAGCTGCCACTTTGACGT
r p21/CIP1	CAGCCACAGGCACCATGTC	ACAGACGACGGCATACTTTGC
r p53	CTGGACGACAGGCAGACTTT	GCACAAACACGAACCTCAAA
r p27	CCGCCTGCAGAAACCTCTT	TCGGCAGTGCTTCTCCAAGT
r p19	ACCCCAAGTGAGGGTTTTCT	GATCCTCTCTGGCCTCAACA

Primers for qPCR (Mouse primers)

Target	**Forward primer**	**Reverse primer**
mKdm3a-1	CCAGGAGAAGACTTCAGAGACATG	GGTGTACTCAGGCAGTGGAATG
mKdm3a-2	TCTCTCTCAGTGTCCAGCTTTGAA	CGTGAGCACCATGGTTTCC
mKdm4c	CCATTCATCCACACCCTCAT	TTGGAACGCAAATACTGGAA
mCenpa	TTCTGTCTTCTGCGCAGTGT	GACCCCAAGGAGGAGACC
mNcapd2	AACCTGCAGTACCATCTCGG	CATGTGCATTCTGCTAGACCA
mNcapg2	CGGTGGTTTTGTCATGGATT	TGGAGATCACTTTGGAAGAGG
mCenpp	GGGAACAGGTACCCTCCAAG	TGTGGAGTGGTGTGAATATCG
mCenpi	TACAGCGACAACAAAGCCTG	GGAGAATGTCAAACCATTTCG
mCenpb	TGAATTCAAGCTGGGAAAGG	CTACAGGCCTCTGCCTCATC
mNcaph	AAGAACATCCTGTTGTCCTCG	TGGGCGCGATTTAAAACTTA
mSmc4	ATGTTCAGTCTGGCCTTTGG	GAAGCCATGGCATTGACTTAG
mSmc2	GCCATGCAGTCCATCTGTTA	AACCAAGCGCAAAGAGCTAC
mp21	GTGTGCCGTTGTCTCTTC	AATCTTCAGGCCGCTCAG
mp53	CGACCTATCCTTACCATCATC	AACTCTAAGGCCTCATTCAGC
mBax	GGAGCAGCTTGGGAGCG	AAAAGGCCCCTGTCTTCATGA
mGADD34	CCCGAGATTCCTCTAAAAGC	CCAGACAGCAAGGAAATGG
mSuv39H1	GCTCTGCCTCCTCTGAGGTAA	TCTCTGCATCTTCCGCACTA

mCenpu	ATCTGTGTCTGTGTGTCCGC	AGACACCAGCAACCCAAAGT
mHjurp	CAGAGGCTTCTCTCATCGCT	TTAAATGGGCAAGCTCCAGA

Primers for ChIP

Target	**Forward primer**	**Reverse primer**
h5S Ribosomal DNA (Chen et al., 2014)	ACGCTGGGTTCCCTGCCGTT	TGGCTGGCGTCTGTGGCACCCGCT
hSatellite 2 (Chen et al., 2014)	TCGCATAGAATCGAATGGAA	GCATTCGAGTCCGTGGA
hD4Z4 (Chen et al., 2014)	CAGGCCTCCTGGCTGCACCT	TGAGCCCCGGCCGGAA TTTCA
h17 alphoid (Chen et al., 2014)	CAACTCCCAGAGTTTCACA TTGC	GGAAACTGCTCTTTGAAAAGGAACC
h21-I alphoid a (Chen et al., 2014)	CTAGACAGAAGCCCTCTCAG	GGGAAGACA TTCCCTTTTTCACC
h21-I alphoid b (Chen et al., 2014)	GTAGTTTGTGGAAGTGGAC	CTGAGAATGCTGCTGTCTACC
hX alphoid a (Chen et al., 2014)	AGA TTTGGACCGCTTTGAGGC	CCGTTCAGTTATGGGAAGTTGA
hX alphoid b (Chen et al., 2014)	CCACAGAAAAACTAAACTGAAGC	GGCTTTCAGGCCTTTTCCACCAC
p15 promoter (Feng et al., 2014)	CTGCCTGGGGATGAATTTAAC	GGTTTCACTGTGGAGACGTTG
p21 promoter (Ohzeki et al., 2012)	TGTGTCCTCCTGGAGAGTGC	CAGTCCCTCGCCTGCGTTG
LMNB1 promoter (Piva et al., 2015)	GTCACCCTCGTCTTGCATTT	GCGTTTAGAGGAACGGAGAA
CENPA promoter (Sidler et al., 2014)	CCTTGGTGTTATGCTCTGGGAAG	GGGCTGTTACTGTTTTCTCAGGTTG
SUV39H1 promoter (Wang et al., 2016)	GCAACTTGAGGACGTGACAG	CCAGCTGTGATTCCTGACAA
KDM3A promoter (Wang et al., 2005)	CTTTCCTGTGAGATTCTTCCGCCA	CCGCGAAATCGGTTATCAACTTTGGG
KDM4C promoter (Wang et al., 2005)	TCCTTCTACGCGAGTATCTTTCCC	GTCACGTGGGCTTACAAACAGCTT

Supplementary Table S3. Antibodies used in this study, Related to Figure 1 to Figure 7

Antibody name	Company	Catalogue number	Isotype
Mono-Methyl-Histone H3 (Lys9) (D1P5R) Rabbit mAb	Cell Signaling Technology	14186	Rabbit
Di-Methyl-Histone H3 (Lys9) (D85B4) XP/TM Rabbit mAb	Cell Signaling Technology	4658	Rabbit
Tri-Methyl-Histone H3 (Lys9) (D4W1U) Rabbit mAb	Cell Signaling Technology	13969	Rabbit
Di/Tri-Methyl-Histone H3 (Lys9) (6F12) Mouse mAb	Cell Signaling Technology	5327	Mouse
Pan-Methyl-Histone H3 (Lys9) (D54) XP Rabbit mAb	Cell Signaling Technology	4473	Rabbit
Histone H3 (D1H2) XP Rabbit mAb	Cell Signaling Technology	4499	Rabbit
Phospho-Histone H2A.X (Ser139) Antibody	Cell Signaling Technology	2577	Rabbit
53BP1 Antibody	Novus	NB100-304	Rabbit
p21 Waf1/Cip1 (DCS60) Mouse mAb	Cell Signaling Technology	2946	Mouse
p21 (F-5)	Santa Cruz Biotechnology	sc-6246	Mouse
p53 (N-19)	Santa Cruz Biotechnology	sc-1314	Goat
p53 (1C12) Mouse mAb	Cell Signaling Technology	2524	Mouse
Lamin A/C (H-110)	Santa Cruz Biotechnology	sc-20681	Rabbit
p15 (C-20)	Santa Cruz Biotechnology	sc-612	Rabbit
HP1γ	Cell Signaling Technology	2619	Rabbit

Phospho-mTOR (Ser2448)	Cell Signaling Technology	5536	Rabbit
Phospho-Rb (Ser807/811) Antibody	Cell Signaling Technology	9308	Rabbit
Rb (4H1) Mouse mAb	Cell Signaling Technology	9309	Mouse
Lamin B1	abcam	ab16048	Rabbit
PCNA (PC-10)	Santa Cruz Biotechnology	sc-56	Mouse
β-tubulin monoclonal antobody	ImmunoWay Biotechnology	YM3139	Mouse
β Tubulin (H-235)	Santa Cruz Biotechnology	sc-9104	Rabbit
Anti-β-Actin mouse mAb	Sigma	A1978	Mouse
β-Actin (D6A8) Rabbit mAb	Cell Signaling Technology	8457	Rabbit
KDM3A (T-14)	Santa Cruz Biotechnology	sc-107656	Goat
KDM3A Polyclonal anitbody	Proteintech	12835-1-AP	Rabbit
Anti-KDM3A / JHDM2A antibody [14F8]	abcam	ab91252	Mouse
Anti-JMJD1A antibody	abcam	ab106456	Rabbit
KDM4C antibody	Bethyl	A300-885A	Rabbit
KDM4C polyclonal antibody	Novus	NBP1-49600	Rabbit
Anti-SUV39H1, clone MG44	Merck Millipore	05-615	Mouse
Anti-KMT1A/SUV39H1antibody	abcam	ab155164	Rabbit
Anti-CENPA antibody [3-19]	abcam	ab13939	Mouse
Anti-HJURP, clone 144K/B1	Merck Millipore	MABE441	Mouse
NCAPD2 Polyclonal antibody	Proteintech	13382-1AP	Rabbit
Anti-NCAPG2 antibody	abcam	ab70350	Rabbit

Transparent Methods

Isolation and characterization of MSCs

The use of human bone marrow and human umbilical cord for MSC isolation were approved by Joint CUHK-NTEC Clinical Research Ethics Committee (ethical approval code: CRE-2011.383, CRE-2010.248 and CRE-2015.018). Clinical specimens were collected in operation theatre, transported to clean room (ISO Class 7; Certified by NEBB) and immersed in Dulbecco's Phosphate Buffered Saline (DPBS) containing 10% P/S during removal of surrounding tissues/muscles/vessels under dissecting microscope (Nikon). The tissues were washed with DPBS twice thoroughly and cut into small pieces and cultured in Knockout DMEM (KO-DMEM, Cell Treatment Therapy, CTS, grade) supplemented with 10% FBS, 1% P/S (CTS) and 1% glutamax (CTS). For the adult bone marrow aspirate, MSCs were isolated by gradient centrifugation in Ficoll®-Paque PREMIUM 1.073 (GE Healthcare, Chicago, Illinois). The mononuclear cells were cultured in α-MEM supplemented with 10% FBS and 1% P/S. At confluence, the cells were trypsinized by TrypLE (CTS), and subjected to either passaging or cryopreserved in 5% DMSO (Sigma Aldrich, 30% FBS, 5% DMSO and 65% KO-DMEM) freezing medium. These MSCs were characterized according to ISCT (2006) minimal criteria. Reagents for cell culture were purchased from Gibco, Life Technologies. Unless otherwise specified, all chemicals were purchased from Sigma-Aldrich. Three hUCMSCs lines (hUC009, hUC011, hUC013) and three hBMSCs lines (hBM001, hBM003, hBM005) were used for functional study. BMSCs derived from nine young (13- to 35-year-old) and five old (52- to 61-year-old) individuals at passage 3 were collected for western blot analyzing the protein expression of senescence markers. Detailed information of this batch of BMSCs is shown in supplementary Table S1.

For primary rat BMSCs isolation, BM was harvested and pooled by flushing the tibias and femurs of rats with α-MEM supplemented with 10% FBS and 1% penicillin-streptomycin in 50ml tubes, and centrifuged at 1500rpm for 5mins. Then cell pellets were re-suspended and cultured in 75 mm^2 flask with complete α-MEM. Medium was changed after 24h and 48h, and adherent cells were expanded after 4 days when cells reached 80%-90% confluence. Phenotype analysis of surface markers was done at passage 2 based on two positive markers CD90, CD54 and two negative markers CD45 and CD34 by FACS. Mouse BMSCs were isolated from bone marrow and compact bone, and the detailed protocols were described previously (Soleimani and Nadri, 2009; Zhu et al., 2010). Compact bone pieces were seeded into 24-well plates and mouse BMSCs derived from compact bone pieces were used for immunofluorescence staining and western blot. Mouse BMSCs collected from bone marrow were used for RNA extraction and real time PCR.

Cell treatment in vitro

To establish replicative senescence model, primary human UCMSCs (Passage 3) or BMSCs (Passage 3) were passaged when cells were grown to 90% confluence. The cells were split in 1:3 and then collected at different passage numbers for cell functional analyses and biochemical analyses. To establish DNA damage-induced cellular senescence, early passage hUCMSCs (p6-p8) were treated with Doxorubicin (Selleckchem, Houston, TX, USA) at 5×10^{-8}M. Samples were treated with Doxorubicin for indicated time points and collected at 0, 3, 7, 10, 12, 24, 36 and 48h for Western blot and Immunofluorescence staining. For IOX1 treatment, hUCMSCs at p6-p8 were treated with IOX1 (Selleckchem, Houston, TX, USA) at different concentrations (20, 50, 70, 100μM) for 3 days, and then harvested for MTT, Western blot, qPCR assay and

β-Gal staining. For ChIP-qPCR assay, hUCMSCs at passage 6-8 were treated with IOX1 at the concentration of 70μM for 1 day, and then fixed with 1% formaldehyde and harvested for ChIP-qPCR assay. For IOX1 treatment during DOX-induced DNA damage, hUCMSCs at p6-p8 were pre-treated with IOX1 (50μM) for 2 days, treated with Doxorubicin at 5×10^{-8} M for 10 hours, and then harvested for Immunofluorescence staining.

β-Gal Staining

We used a β-Gal Staining assay kit (Cell Signaling Technology, Danvers, MA, USA) following the manufacturer's protocol. Briefly, cells were washed with PBS twice and fixed with 1 × Fixative Solution for 10 min at room temperature. After washing, the cells were incubated at 37°C with fresh β-Galactosidase Staining Solution [pH 6.0]. The experiment was repeated three times and the number of cells expressing β-Gal was calculated.

Clonogenic assay

2000 cells were seeded in 60 × 15mm cell culture dish, and cultured for continuous 10 days. After that, cells were fixed with cooled absolute methanol for 2 minutes and stained for 5 minutes with 1% crystal violet aqueous solution.

siRNA-mediated knockdown and plasmid transfection

siRNA pools targeting KDM3A and KDM4C were purchased from Invitrogen (Life Technologies, Carlsbad, USA). KDM3A, KDM4C and NCAPD2 plasmids (pcDNA3.1(+)-KDM3A, pcDNA3.1(+)-KDM4C and pcDNA3.1(+)-NCAPD2) were purchased from Viral therapy Technologies Co. Ltd (Wuhan, China). hUCMSCs (p6-

p8) were transfected with siRNAs or plasmids using Lipofectamine® 2000 Transfection Reagent (Life Technologies). 48 - 72 hours after transfection, knockdown or overexpression efficiency were determined by quantitative real-time PCR or Western blot, and other molecular analyses including RNA-seq analyses, detection of downstream targets and ChIP assays. siRNAs used in this study are: KDM3A siRNA ID: HSS125107, HSS125109, HSS183294; KDM4C siRNA ID: HSS118146, HSS177158, HSS177159. For cell functional analyses, early passage hUCMSCs (P6-8) were pre-treated with siRNAs mixture (siKDM3A and siKDM4C) or scrambled siRNA for two days, and then treated with Doxorubicin at 5×10^{-8} M for 12 hours. Samples were then collected for immunofluorescent staining and β-Gal staining. For overexpression experiments, early passage hUCMSCs (p6-8) were transfected with KDM3A, KDM4C or NCAPD2 or control vectors for 24 hours, and then treated with medium containing 5×10^{-8}M Doxorubicin for another 12 hours.

Lentiviral shRNA knockdown

Stable knockdown of KDM3A or KDM4C cells was achieved by lentiviral transduction of pLVX- ShRNA-Puro-ZsGreen-hKDM3A-1, 2, 3 or pLVX-ShRNA-Puro-ZsGreen-hKDM4C-1, 2, 3 (Viraltherapy Technologies, Wuhan, China) or control virus pLVX- ShRNA-Puro-ZsGreen. After 48 h transduction, the transduced cells were propagated for two continuous passages, and then sorted by Flow Cytometer (BD FACSAria II Cell sorter) to select out positively-transduced cells based on ZsGreen positivity. shRNA targeting sequences are shown below: shKDM3A-1：5‘- CCT CCG GAA TCT CTT GAA TTC TTC T-3’; shKDM3A-2：5‘- GCA GCT GTA CTC AGC CTA AGA-3’; shKDM3A-3：5‘- GCA GGT GTC AAT AGT GAT AGC-3’; shKDM4C-1：5‘-GAG GAG TTC CGG GAG TTC AAC AAA T-3’; shKDM4C-2：

5‘- GGA GTT CAA CAA ATA CCT TGC-3’; shKDM4C-3：5‘- GCA GGT GGA GCA GAA TTT ATC-3’.

Real-time Reverse Transcriptase-Polymerase Chain Reaction (qRT-PCR)

Total RNA was isolated from MSCs using Trizol reagent (Life Technologies). 2 μg RNA was used to synthesize cDNA with oligo (dT) and reverse transcriptase, following the manufacturer’s protocol (Promega, Madison, WI, USA). Real-time RT-PCR reactions were performed using the SYBR Green PCR kit (Takara, Kusatsu, Shiga, Japan) and a 7500 Fast Real-Time PCR System (Applied Biosystems, CA, USA). The primers used for specific genes is presented in Supplementary Table S2.

RNA-Seq and Data processing

The construction of RNA-seq library and the sequencing were done by Beijing Genomics Institute (Shenzhen, China). Briefly, total RNA from treated samples was extracted using Trizol reagent (Life Technologies, Carlsbad, CA, USA). mRNA samples were prepared for RNA-Seq analysis using the Illumina TruSeq RNA Sample Prep Kit V2 (Illumina, San Diego, CA) according to the manufacturer's protocol. To produce the final cDNA libraries, universal adapters were ligated to the cDNA fragments followed by PCR amplification. The quality of sequencing library was tested using Agilent 2100 bioanalyzer. For enrichment of cDNA in the library, polymerase chain reaction (PCR) was carried out which selectively amplified those fragments with adapter molecules on both ends. The established cDNA libraries were applied to HiSeq2000 platform (TruSeq SBS KIT-HS V3, Illumina) with paired-end sequencing length of 90 bp. The levels of gene expression level and the differentially expressed genes were analyzed using the method described by Audic and Claverie(Audic and

Claverie, 1997). Levels of gene expression were calculated using the reads per kilobase million (RPKM) method. In cases where more than one transcript was found for a gene, the longest read was used to calculate its expression level and coverage. The significantly differentially expressed genes (DEG) were determined at a threshold false discovery rate (FDR) ≤ 0.05 and the absolute value of log2ratio ≥ 1 or ≤ 1. All DEGs were mapped to GO terms in the database (http://www.geneontology.org/); gene numbers have been calculated for every term, using a hypergeometric distribution compared with the genome background. We used Partek software to conduct GO analysis and mapped all the DEGs obtained from these libraries (p value < 0.05) to GO database, to classify for enriched GO terms, and analyze the DEGs based on the Organelle organization and Chromosome organization. Genomic data generated during the study are available in a public repository GEO (GSE133098).

Western Blot Analysis

Cells were lysed and protein was extracted using RIPA (Pierce, Rockford, IL, USA) plus protease inhibitor cocktail (Thermo Fisher, Waltham, MA, USA), and protein concentrations were determined using the BCA assay (Bio-Rad, Richmond, CA, USA). Aliquots of protein lysates were separated on SDS-6, 8, 10, 12% polyacrylamide gels and transferred onto polyvinylidene difluoride (PVDF) membrane, which was blocked with 4% blotting-grade milk in TBST (20 mM Tris–HCl [pH 7.6], 137 mM NaCl, and 1% Tween 20). The membrane was then hybridized with the indicated primary antibodies followed by the corresponding secondary antibodies, and then detected using ECL (GE). Membranes were exposed to X-ray film (Fuji Photo Film, Tokyo, Japan) to visualize the bands. The antibodies used in this study are listed in Supplementary Table S3.

Chromatin immunoprecipitation (ChIP) assay

We used a ChIP assay kit (Merck Millipore, Darmstadt, Germany) following the manufacturer's protocol. Briefly, cells were incubated with 1% formaldehyde (Sigma-Aldrich, MO, USA) for 10 minutes at 37°C, and then quenched of formaldehyde using 2.5M glycine. Each ChIP reaction was performed using 6.0×10^6 cells. For DNA precipitation, we added 3-5 μg ChIP-grade antibodies against H3K9me1, H3K9me2, H3K9me3, KDM3A and KDM4C. The precipitated DNA samples were quantified by qPCR with primers targeting on special sites. Primers for ChIP assay are presented in Supplementary Table S2.

Immunofluorescence staining

Cells seeded on slides were fixed in 4% paraformaldehyde for 10 min, and were washed with PBS for three times. The immunofluorescence staining in detail was performed as previously described(Huang et al., 2016). The antibodies used for immunofluorescence staining were listed in Supplementary Table S2. The Alexa FluorSeries from Invitrogen were used as secondary antibodies. Images were taken using a confocal system with inverted microscope (Olympus FV1000) and analyzed with FluoView 4.2a. For all quantitative analyses, images were collected using the same acquisition parameters to facilitate fluorescence intensity comparisons between groups. Corrected total cell fluorescence intensity (CTCF) was defined as area × (mean intensity−background intensity). For DNA damage foci analysis, all experiments were repeated three times, each experiment were set up for triplicates. 5 fields per slide were analyzed under the microscope and no less than 100 cells were analyzed for quantification data.

Transmission electron microscopy (TEM)

hUCMSCs transfected with KDM3A or KDM4C plasmids after 24h were harvested, then fixed and processed for TEM, as described previously(Stolz et al., 1999). After dehydration, thin sections (70 nm) (Leica UCT7) were stained with uranyl acetate and lead citrate for observation under a Transmission Electron Microscope (Hitachi H-7700).

The establishment of Ovariectomized (OVX) rat model and isolation of rat BMSCs from OVX rat bone marrow

All animals were provided by the Laboratory Animal Service Center of the Chinese University of Hong Kong. They were maintained in an air-conditioned room with controlled temperature of 24 ± 2 °C and humidity of 55 ± 15%, in a 12 h light/darkness cycle regulation and were fed laboratory chow and water *ad libitum*. All animal experiments were conducted in accordance with the University Laboratory Animals Service Center's guidelines on animal experimentation with approval from the Animal Ethnics Committee of the University. Thirty 6 month-old Spraque-Dawley female rats were used. 24 rats were subject to ovariectomy, and 6 received sham surgery. Briefly, a 1.5 cm skin incision was made to expose the dorsolateral abdominal muscles and ligation was performed at the distal uterine horn to remove the ovarian tissue completely. 6 animals with sham surgery were sacrificed at week 0. 6 animals per group in the OVX treatment were euthanized at week 3, 6, 9 and 12 post-surgeries. Serum, uterus, body weight, lumber vertebra, femur, and tibia were collected at the time of euthanization, and the 5th lumbar vertebras (LV5) were dissected for measurement of trabecular micro-CT analysis. For primary rat BMSCs isolation, BM was harvested and

pooled by flushing the tibias and femurs of sham and OVX female rats (n = 6 for every group) and cultured in α-MEM supplemented with 10 % FBS, Glutamax (2 mg/ml) and 1 % penicillin-streptomycin. Medium was changed after 24h and 48h, and adherent cells were expanded after 4 days. Phenotype analysis of surface markers was done at passage 2 based on two positive markers CD90, CD54 and two negative markers CD45 and CD34 by FACS. Cells at passage 3 were used for western blot and qPCR assay.

Micro-computed Tomography (micro-CT) Scanning

The OVX rats LV5s and mouse femurs were scanned using a desktop preclinical specimen micro-CT (uCT-35, Scanco Medical, Bassersdorf, Switzerland). Briefly, the vertebral bodies or femurs were aligned perpendicularly to the scanning axis for a total scanning length of 6.0 mm at custom isotropic resolution of 8-µm isometric voxel size with a voltage of 70 kV p and a current of 114 µA. Three-dimensional (3D) reconstructions of mineralized tissues were performed by an application of a global threshold (211 mg hydroxyapatite/cm3), and a Gaussian filter (sigma = 0.8, support = 2) was used to suppress noise. A volume of interest (VOI) containing only trabecular bone within the vertebral body extracted from the cortical bone with 1.80-mm thick (150 slices) was acquired from both cranial and caudal growth plate-metaphyseal junctions. The three-dimensional reconstructed images were used directly to quantify microarchitecture, and the morphometric parameters including bone volume fraction (BV/TV), trabecular number (Tb.N, 1/mm) and trabecular separation (Tb.Sp, mm) were calculated with the image analysis program of the micro- CT workstation (Image Processing Language v4.29d, Scanco Medical, Switzerland)

Kdm3a$^{-/-}$ knockout mice

The *Kdm3a*$^{-/-}$ mice was created by Prof. Xu Jianming's lab at the Baylor College of Medicine, Houston, TX (Liu et al., 2010). Bone tissues were derived as described before for CT scanning and western blot analysis. BMSCs were derived from 6 month-old female WT (n=3) and *Kdm3a*$^{-/-}$ knockout mice (n=3), and then subjected to 5×10^{-8} Doxorubicin. Samples were collected at different time points for real-time and immunofluorescence staining. For the rescue experiment, isolated BMSCs from WT (n=3) and *Kdm3a*$^{-/-}$ knockout mice (n=3) were subjected to 5×10^{-8} Doxorubicin treatment and simultaneously KDM3A plasmid transfection. Treated samples were collected at 0, 3, 7, and 10 hours after treatment for immunofluorescence staining and β-Gal staining.

Statistical analysis

Data are presented as mean ± SEM. At least three independent experiments were performed for each assay. Statistical differences were calculated with the two-tailed Student's t test when comparing two conditions. One-way ANOVA and Tukey's post hoc test were used when there were more than two groups. We used Wilcoxon/Mann-Whitney method when normal data distribution cannot be assured. Results were considered statistically significant at *P < 0.05, ** P < 0.01, *** P < 0.001 and **** for P < 0.0001.

Supplemental References:

Audic, S., and Claverie, J.M. (1997). The significance of digital gene expression profiles. Genome Res 7, 986-995.

Chen, X., Iliopoulos, D., Zhang, Q., Tang, Q., Greenblatt, M.B., Hatziapostolou, M., Lim, E., Tam, W.L., Ni, M., Chen, Y., et al. (2014). XBP1 promotes triple-negative breast cancer by controlling the HIF1alpha pathway. Nature 508, 103-107.

Feng, Y., Wu, H., Xu, Y., Zhang, Z., Liu, T., Lin, X., and Feng, X.H. (2014). Zinc finger protein 451 is a novel Smad corepressor in transforming growth factor-beta signaling. J Biol Chem 289, 2072-2083.

Huang, B., Cheng, X., Wang, H., Huang, W., Wang, D., Zhang, K., Zhang, H., Xue, Z., Da, Y., and Zhang, N. (2016). Mesenchymal stem cells and their secreted molecules predominantly ameliorate fulminant hepatic failure and chronic liver fibrosis in mice respectively. Journal of translational medicine 14, 1.

Liu, Z., Zhou, S., Liao, L., Chen, X., Meistrich, M., and Xu, J. (2010). Jmjd1a demethylase-regulated histone modification is essential for cAMP-response element modulator-regulated gene expression and spermatogenesis. J Biol Chem 285, 2758-2770.

Ohzeki, J., Bergmann, J.H., Kouprina, N., Noskov, V.N., Nakano, M., Kimura, H., Earnshaw, W.C., Larionov, V., and Masumoto, H. (2012). Breaking the HAC Barrier: histone H3K9 acetyl/methyl balance regulates CENP-A assembly. EMBO J 31, 2391-2402.

Piva, R., Lambertini, E., Manferdini, C., Capanni, C., Penolazzi, L., Gabusi, E., Paolella, F., Lolli, A., Angelozzi, M., Lattanzi, G., et al. (2015). Slug transcription factor and nuclear Lamin B1 are upregulated in osteoarthritic chondrocytes. Osteoarthritis Cartilage 23, 1226-1230.

Sidler, C., Li, D., Wang, B., Kovalchuk, I., and Kovalchuk, O. (2014). SUV39H1 downregulation induces deheterochromatinization of satellite regions and senescence after exposure to ionizing radiation. Front Genet 5, 411.

Soleimani, M., and Nadri, S. (2009). A protocol for isolation and culture of mesenchymal stem cells from mouse bone marrow. Nature protocols 4, 102-106.

Stolz, D.B., Ross, M.A., Salem, H.M., Mars, W.M., Michalopoulos, G.K., and Enomoto, K. (1999). Cationic colloidal silica membrane perturbation as a means of examining changes at the sinusoidal surface during liver regeneration. The American journal of pathology 155, 1487-1498.

Wang, G., Yu, Y., Sun, C., Liu, T., Liang, T., Zhan, L., Lin, X., and Feng, X.H. (2016). STAT3 selectively interacts with Smad3 to antagonize TGF-beta signalling. Oncogene 35, 4388-4398.

Wang, I.C., Chen, Y.J., Hughes, D., Petrovic, V., Major, M.L., Park, H.J., Tan, Y., Ackerson, T., and Costa, R.H. (2005). Forkhead box M1 regulates the transcriptional network of genes essential for mitotic progression and genes encoding the SCF (Skp2-Cks1) ubiquitin ligase. Mol Cell Biol 25, 10875-10894.

Zhu, H., Guo, Z.-K., Jiang, X.-X., Li, H., Wang, X.-Y., Yao, H.-Y., Zhang, Y., and Mao, N. (2010). A protocol for isolation and culture of mesenchymal stem cells from mouse compact bone. Nature protocols 5, 550-560.